



CERN-EP-2019-244
28 October 2019

Jet-hadron correlations measured relative to the second order event plane in Pb–Pb collisions at $\sqrt{s_{NN}} = 2.76$ TeV

ALICE Collaboration*

Abstract

The Quark Gluon Plasma (QGP) produced in ultra relativistic heavy-ion collisions at the Large Hadron Collider (LHC) can be studied by measuring the modifications of jets formed by hard scattered partons which interact with the medium. We studied these modifications via angular correlations of jets with charged hadrons for jets with momenta $20 < p_T^{\text{jet}} < 40$ GeV/c as a function of the associated particle momentum. The reaction plane fit (RPF) method is used in this analysis to remove the flow modulated background. The analysis of angular correlations for different orientations of the jet relative to the second order event plane allows for the study of the path length dependence of medium modifications to jets. We present the dependence of azimuthal angular correlations of charged hadrons with respect to the angle of the axis of a reconstructed jet relative to the event plane in Pb–Pb collisions at $\sqrt{s_{NN}} = 2.76$ TeV. The dependence of particle yields associated with jets on the angle of the jet with respect to the event plane is presented. Correlations at different angles relative to the event plane are compared through ratios and differences of the yield. No dependence of the results on the angle of the jet with respect to the event plane is observed within uncertainties, which is consistent with no significant path length dependence of the medium modifications for this observable.

arXiv:1910.14398v1 [nucl-ex] 31 Oct 2019

© 2019 CERN for the benefit of the ALICE Collaboration.

Reproduction of this article or parts of it is allowed as specified in the CC-BY-4.0 license.

*See Appendix A for the list of collaboration members

1 Introduction

A hot, dense liquid of quarks and gluons is created in high energy collisions of heavy ions at the Relativistic Heavy Ion Collider (RHIC) [1–4] and the Large Hadron Collider (LHC) [5–11]. This strongly interacting medium, called the Quark Gluon Plasma (QGP), suppresses colored probes such as quarks and gluons.

Hard parton scatterings occur early in the collision and lead to the production of jets, collimated sprays of particles formed from the fragmentation of the scattered parton. These hard partons lose energy through induced gluon bremsstrahlung and elastic collisions with medium partons as they traverse the QGP, leading to a broadening of the resulting jet and softening of its constituents [12, 13]. This energy loss can be studied with measurements of high transverse momentum hadrons or reconstructed jets. High momentum charged hadron production is suppressed by a factor of approximately five in Au–Au collisions at RHIC [14–16] and up to a factor of nearly ten in Pb–Pb collisions at the LHC [7, 17] relative to that in pp collisions. These measurements are used to constrain the transport coefficient \hat{q} , the squared partonic momentum exchanged with the medium divided by the path length traversed [18] in the QGP.

An enhancement of particle production at low p_T due to medium interactions has been observed with measurements of fragmentation functions, the momentum distributions of particles within the jet [19–21], as well as through broadening in high momentum dihadron correlations [22, 23] and jet-hadron correlations [11, 24–26].

Measurements of correlations allow studies of lower energy jets and of the soft constituents by means of statistical subtraction of the large combinatorial background at lower momenta. Studies of correlations have been limited by methods for background subtraction due to the structures in the background correlated with the signal because of hydrodynamical flow. The recent development of the Reaction Plane Fit (RPF) method enables precision subtraction of the background for both jet-hadron and dihadron correlations [27].

The path length dependence of partonic energy loss can be constrained through measurements of the dependence of azimuthal correlations of high momentum particles or reconstructed jets on the angle of the jet relative to second order event plane of the collision. Because the overlap region of the incoming nuclei for non-central collisions is almond shaped, particles traveling perpendicular to this event plane (out-of-plane) have a longer path length through the medium on average than those traveling in the direction of the event plane (in-plane). Therefore, the suppression of high momentum single particles is expected to be greater in the out-of-plane direction than in-plane [28]. This is also evident in the azimuthal anisotropy of high- p_T single particle [29–32] and jet [33, 34] production relative to the second order event plane. This suppression indicates that there are fewer jets out-of-plane after interactions with the medium, but is not a measure of the properties of the surviving jets relative to that plane. Measurements of dihadron correlations relative to the event plane at RHIC indicate suppression and some broadening [35, 36], but do not exhibit much event plane dependence [37]. Some theoretical studies indicate that jet-by-jet fluctuations in the energy loss may be as important as the path length dependence for some observables, such as azimuthal anisotropies at high momentum and di-jet asymmetries [38–40].

Measurements for the event plane dependence of jet modification can therefore provide insight into the relative importance of path length for partonic energy loss. We present measurements of jet-hadron correlations relative to the event plane in Pb–Pb collisions at $\sqrt{s_{NN}} = 2.76$ TeV using A Large Ion Collider Experiment (ALICE) detector. We first describe the details of the measurement technique and then present the results. We conclude with a discussion of the constraints these measurements provide for models.

2 The ALICE detector

A detailed description of the ALICE detector and its subdetectors can be found in [41]. The detectors used for the present analysis are briefly described in this section. These are the forward scintillator arrays (V0) [42, 43], Inner Tracking System (ITS) [44], the Time Projection Chamber (TPC) [45], and the Electromagnetic Calorimeter (EMCal) [46].

The V0 detector is used for centrality estimation and event plane reconstruction. The V0 system consists of two scintillator arrays located at asymmetric positions, one at a pseudorapidity range of $2.8 < \eta < 5.1$ (V0A) and the other at $-3.7 < \eta < -1.7$ (V0C) [42]. Each set of arrays is made of four radial rings with each ring divided into eight sections in the azimuthal direction [42].

The ITS and TPC detectors provide tracking of charged particles over the full range of azimuth with a pseudorapidity range of $|\eta| < 0.9$. They are located inside the central barrel solenoidal magnet which provides a homogenous field with strength of 0.5 T [47]. The ITS is a cylindrical silicon detector made up of 6 layers located at the center of the main-barrel. The first two layers are the Silicon Pixel Detectors (SPD), followed by two layers of Silicon Drift Detectors (SDD), and two outer layers of Silicon Strip Detectors (SSD) [48]. The TPC surrounds the ITS and is the main detector used for tracking in ALICE. It is filled with a gas mixture of Ne and CO₂ [49]. The transverse momentum and charge of the particles can be inferred from the curvature of the tracks. Combining information from the ITS and TPC allows for the momentum determination of charged particles as low as $p_T \approx 0.15$ GeV/ c up to $p_T \approx 100$ GeV/ c .

Track selection is optimized for track quality, momentum resolution, and nearly uniform azimuthal acceptance, as in [47]. At least three hits in the ITS are required. Tracks without a hit in the SPD are refit to include the primary vertex, reducing the azimuthal dependence of the track reconstruction efficiency while maintaining good momentum resolution. The tracks used in this analysis are required to have 80% of the geometrically allowed space points and at least 70 total space points in the TPC. The tracking efficiency is determined from simulations of the detector response using tracks simulated with HIJING [50] propagated through the detector using GEANT3 [51] and ranges from 80–85% in the momentum range used in this analysis.

The uncertainty on the single track reconstruction efficiency is 4%, with an additional 1% systematic uncertainty due to contamination from secondary tracks [47, 52–54]. This uncertainty is correlated point-to-point and contributes to the scale uncertainty in the correlation functions and yields.

The EMCal is used for the neutral energy reconstruction and triggering. It is a lead-scintillator sampling calorimeter with a pseudorapidity coverage of $|\eta| < 0.7$ and an active azimuthal range of $\Delta\phi = 107^\circ$ in the readout in the 2011 configuration [46, 55, 56]. The EMCal had 11520 towers with transverse size 6 cm \times 6 cm, or approximately twice the effective Molière radius. The relative energy resolution is $0.11/\sqrt{E} + 0.017 + 0.051/E$, where the energy E is measured in GeV [55]. Clusters are formed by combining signals from adjacent towers and each cluster is required to have only one local energy maximum. This analysis uses events triggered by a high energy deposit in a 4×4 region of towers in the EMCal. This trigger configuration has less sensitivity to the underlying event than a trigger configuration with a larger area, often used for jet analyses, because the contribution of the underlying event to the energy is proportional to the trigger area. The raw trigger threshold was multiplicity dependent and corresponded to approximately 4.5–6 GeV in the centrality bin used in this analysis.

Clusters with energy above 3 GeV, which exclude minimally ionizing particles [56], are used in this analysis. Partially formed hadronic showers may still pass this threshold. To avoid overcounting of charged particle p_T , the cluster energies are corrected as in [53]. Tracks are propagated to the average cluster depth in the EMCal and matched to the nearest cluster. If the nearest cluster is within $|\Delta\eta| < 0.015$ in pseudorapidity and $|\Delta\phi| < 0.025$ in azimuth, the cluster most likely arose from a charged hadron. If the cluster energy is at or below the track's momentum, the cluster is not used in the analysis, while if

the cluster energy is above the track's momentum, the track momentum is subtracted from the cluster energy [53].

3 Method

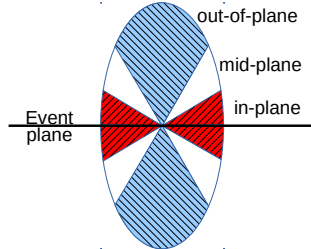


Figure 1: Jet-hadron correlations are measured for jets in three regions relative to the $n = 2$ event plane, which is transverse to the direction of the beams. These regions include in-plane ($|\psi - \phi_{\text{jet}}| < \pi/6$) shown in red, mid-plane ($\pi/6 < |\psi - \phi_{\text{jet}}| < \pi/3$) shown in white, and out-of-plane ($|\psi - \phi_{\text{jet}}| > \pi/3$) shown in blue.

The data used in this analysis were collected during the 2011 run [41] from 0.5M 30–50% central Pb–Pb collisions at $\sqrt{s_{\text{NN}}} = 2.76$ TeV. It was additionally required to be triggered by a high energy deposit in a 4×4 region of towers in the EMCal [56]. Procedures for selection and reconstruction of tracks from charged particles, identification of calorimeter clusters, and jet reconstruction are as in [47] and are summarized in sec. 3.1. Estimates of the distributions of corrected jet energies are also reported here. The experimentally reconstructed second order symmetry plane is called the second order event plane, referred to as the “event plane” later in the text for simplicity. Centrality determination and event plane reconstruction is discussed in sec. 3.2. Jets from triggered events are correlated with all charged tracks in azimuth ($\Delta\phi = \phi_{\text{jet}} - \phi_{\text{assoc}}$) and pseudorapidity ($\Delta\eta = \eta_{\text{jet}} - \eta_{\text{assoc}}$), as discussed in sec. 3.3. The distributions of these associated tracks relative to the trigger jet are measured in three bins in the angle between the trigger jet and the event plane, in-plane ($|\psi - \phi_{\text{jet}}| < \pi/6$), mid-plane ($\pi/6 < |\psi - \phi_{\text{jet}}| < \pi/3$), and out-of-plane ($|\psi - \phi_{\text{jet}}| > \pi/3$) bins, as shown in fig. 1. The analysis is restricted to 30–50% central Pb–Pb collisions because this is where the event plane resolution is highest and therefore the analysis will be most sensitive to any path length dependencies. The subtraction of the combinatorial background using the RPF method [27] is discussed in sec. 3.4. The determination of the yields and the widths is discussed in sec. 3.5. The possible impact of the finite event plane resolution on the signal is discussed in sec. 3.6.

3.1 Jet reconstruction and energy distribution

Tracks and corrected EMCal clusters are clustered into jets using the anti- k_T algorithm with a resolution parameter $R = 0.2$ in the FastJet package [57]. Jet transverse momenta are calculated as the scalar sum of their constituent transverse momenta using a boost-invariant p_T recombination scheme. Tracks are assumed to be pions and clusters to arise from massless particles. In order to suppress contributions from combinatorial jets and the contribution of uncorrelated background to the jet energy, jets are reconstructed with constituents above $p_T > 3$ GeV/ c and are required to have an area of at least 0.08 calculated using ghost particles as described in [57]. Jets are required to be within $|\eta_{\text{jet}}| < 0.5$ and $1.6 < \phi_{\text{jet}} < 2.9$ so that the entire jet is contained within the EMCal acceptance.

Small jets are used to reduce the impact of the background, as background contributions scale with R^2 . Additionally, to further suppress contributions of the background to the energy and to match trigger conditions [46], the jets are required to contain a cluster with transverse energy larger than 6 GeV. We note that this requirement leads to a selection of biased jets, explicitly biasing the near-side. The

away-side, in contrast, is not explicitly biased, although it is unlikely to be a random sample of the jet population. With these constituent cuts, the background contribution to the energy is negligible using estimates of the background per unit area as in [58]. The background contribution to the energy is therefore not subtracted from the jets, although any residual contribution would be included in the energy distribution estimation. The jet energy is not corrected for detector effects, but the distribution of particle level jet energies in the sample is estimated using PYTHIA6 [59] Tune A [60] simulations embedded at detector level into data measured in Pb–Pb collisions and matched back to generator level.

Detector effects such as the single track reconstruction efficiency, momentum resolution in the tracking detectors and energy resolution in the calorimeter combined with contributions from particles which are not directly observed, such as neutrons and K_L^0 , and contributions from the background lead to a finite energy resolution. This means that when jet-hadron correlations are measured at a particular jet p_T , the distribution of true jet momenta is broad. A full correction for this effect would require two dimensional unfolding with jet-hadron correlations measured for several jet momenta. The current statistics do not allow for such measurements. Instead, we estimate the distribution of true jet energies and focus on comparisons between jets at different angles relative to the event plane to enable the highest precision search for path length dependence allowed by the currently available data.

The kinematic selection of tracks and clusters used in jet finding is chosen to suppress contributions from the combinatorial background and reduce smearing of the jet energy due to the large combinatorial background. With these kinematic selections, the background density is negligible and showed no event plane dependence. Given that no event plane dependence is observed in the signal, this also means that the resolution of the jet axis does not vary with the angle of the jet relative to the event plane.

PYTHIA6 TuneA [59, 60] simulations of pp collisions with jets are embedded at detector level into 30–50% Pb–Pb data. The embedded events are analyzed with the same parameters and cuts as the data analysis, including the jet constituent and cluster biases, while the generator level jets are measured for $p_T > 5$ GeV/c. The generator level jets are first matched geometrically to PYTHIA detector level jets, and then the detector level jets are geometrically matched to jets found within $R = 0.2$ in the embedded event, with the additional requirement the associated generator level jet distribution is measured. Each such distribution is normalized within the region $20 \leq p_T < 100$ GeV/c where fluctuations are minimized and, assuming that the jet energy distribution in the data is the same as that provided by PYTHIA6, describes the generator level jet distribution that corresponds to the measured detector level jet distribution, shown in fig. 2. The uncertainty on the jet energy scale is 2.6% and the jet energy resolution, which is also encoded in the response matrix, is around 20% for the jets selected in this analysis [53]. There are slight differences in the for jets reconstructed with $p_T \leq 20$ GeV/c for jets at different angles relative to the event plane due to a low momentum embedded jet overlapping with a another jet in the Pb–Pb data. Since there are more jets in-plane than out-of-plane in the data, this leads to an apparent difference in the reconstructed jet spectra. Otherwise there are no significant differences between jets at different angles relative to the event plane.

3.2 Centrality determination and event plane reconstruction

Centrality is determined from the sum of the energy deposition [42] in the V0 scintillator tiles, as described in [61]. The centrality of the collision is reported as percent ranges of the total hadronic cross section, with lower percentiles referring to the most central (largest multiplicity) events [61]. The second order event plane $\Psi_{EP,2}$ is reconstructed using the V0 following the procedure in [33] by combining signals from the V0A and V0C arrays [43]. The separation in pseudorapidity between the measurement of the signal and the measurement of the event plane suppresses the contribution from the jet signal to the event plane determination [33].

The reaction plane is defined by the beam axis and the vector between the centers of the two incoming nuclei. Additional asymmetries in the distribution of nucleons within the overlap region, generally

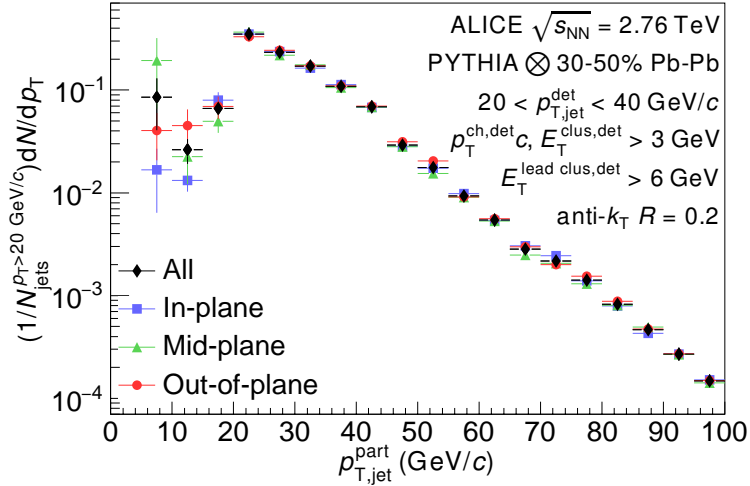


Figure 2: The generator level jet probability distribution corresponding to jets measured with p_T between 20–40 GeV/c for PYTHIA events embedded in 30–50% central Pb–Pb collisions. Generator level jets are required to have $p_T > 5$ GeV/c. The distribution is measured for each angle relative to the event plane, as well as the sum of all angles.

quantified by a harmonic decomposition, generate symmetry planes at all orders ($n > 0$) [62, 63]. If the nucleons were in their average positions and there were no fluctuations in interactions between nucleons, the reaction plane would correspond to the second order symmetry plane, $\Psi_{EP,2}$. The experimentally reconstructed symmetry planes are called event planes. For simplicity, we refer here to the experimentally reconstructed second order event plane as the event plane. As explained below, we do not correct the signal for the difference between the event and symmetry planes because no event plane dependence is observed in this measurement. Corrections for the event plane resolution will increase differences between results at different angles relative to the event plane but will not induce any event plane dependence if there is none in the uncorrected results. We discuss the impact of the event plane resolution in sec. 3.6. The impact of the dijets on the event plane reconstruction was studied in [33] and found to be negligible.

The event plane is also extracted using TPC tracks in order to determine the event plane resolution. The n -th order event plane can be calculated from the charged particle azimuthal distribution by [64]:

$$\Psi_{n,EP} = \left(\arctan \frac{\sum_i w_i \sin(n\phi_i)}{\sum_i w_i \cos(n\phi_i)} \right) / n, \quad (1)$$

where the sum is over all particles in the event, ϕ_i is the azimuthal angle of the i -th particle, and w_i is the weight of the i -th particle. For measurement of the event plane with the V0, the sum is over all of its sectors and the weights are equal to the amplitude of the respective sector in the V0, which is proportional to the local multiplicity. A calibration and recentering procedure following [33] is applied to remove any bias introduced by non-uniform acceptance of the V0 system. For measurement in the TPC, tracks are given equal weights ($w_i = 1$) and the acceptance is nearly uniform. Track selection is the same as that described in sec. 3 except the transverse momentum range is restricted to $0.15 < p_T < 5.0$ GeV/c. More details of the procedure can be found in [33].

Due to the finite multiplicity of each event, there will be a difference between the symmetry plane and the reconstructed event plane. This difference is quantified by the event plane resolution

$$\mathfrak{R}_n = \langle \cos(n[\Psi_{n,EP} - \Psi_n]) \rangle. \quad (2)$$

where Ψ_n is the true angle and $\Psi_{n,EP}$ is the measured angle of the n th order event plane. To evaluate the event plane resolution directly from data, this analysis uses three sub-events, comparing the event planes measured in the full V0, measured in the TPC using tracks at positive pseudorapidities, and measured in the TPC using tracks at negative pseudorapidities. We can express the n th order resolution of the full V0, \mathfrak{R}_n^{V0} [64, 65], of the second order event plane by

$$\mathfrak{R}_n^{V0} = \langle \cos(n[\Psi_{2,EP}^{V0} - \Psi_2]) \rangle = \sqrt{\frac{\langle \cos(n[\Psi_{2,EP}^{V0} - \Psi_{2,EP}^{TPC,\eta>0}]) \rangle \langle \cos(n[\Psi_{2,EP}^{V0} - \Psi_{2,EP}^{TPC,\eta<0}]) \rangle}{\langle \cos(n[\Psi_{2,EP}^{TPC,\eta>0} - \Psi_{2,EP}^{TPC,\eta<0}]) \rangle}} \quad (3)$$

where $\Psi_{2,EP}^{V0}$, $\Psi_{2,EP}^{TPC,\eta>0}$, and $\Psi_{2,EP}^{TPC,\eta<0}$ are the second order event planes calculated using the three different sub-events, and Ψ_2 is the true angle of the second order symmetry plane. Fits to the Fourier decomposition of the correlated background are performed up to $n = 4$ and are measured relative to the event plane. Thus, event plane resolution corrections $\mathfrak{R}_2(\psi_2)$ and $\mathfrak{R}_4(\psi_2)$ are needed to correct these terms for the finite precision of the second order event plane measured in the V0 system, as discussed in sec. 3.4. The event plane resolution for the 30-40% and 40-50% centrality ranges are combined by weighting the two samples by the number of corresponding events of each. The event plane resolutions $\mathfrak{R}_2(\psi_2)$ and $\mathfrak{R}_4(\psi_2)$ for the analyzed 30-50% event sample are 0.73 and 0.44, respectively, with negligible uncertainties.

3.3 Jet-hadron correlations

The distribution of charged particles relative to $20 < p_T^{\text{jet}} < 40$ GeV/ c reconstructed jets is measured in azimuth ($\Delta\phi$) and pseudorapidity ($\Delta\eta$) as

$$\frac{1}{N_{\text{trig}}} \frac{d^2 N_{\text{assoc}}}{d\Delta\phi d\Delta\eta} = \frac{1}{N_{\text{trig}}} \frac{1}{a(\Delta\phi, \Delta\eta) \varepsilon(p_T^{\text{assoc}}, \eta^{\text{assoc}})} \frac{d^2 N_{\text{meas}}}{d\Delta\phi d\Delta\eta} \quad (4)$$

where N_{trig} is the number of trigger jets, $\varepsilon(p_T^{\text{assoc}}, \eta^{\text{assoc}})$ is the product of the single track reconstruction efficiency and acceptance, and $a(\Delta\phi, \Delta\eta)$ dominantly corrects for the pair acceptance. The distributions are determined in bins of centrality, associated hadron transverse momentum (p_T^{assoc}), and bins of the trigger jet angle relative to the event plane.

The correction $a(\Delta\phi, \Delta\eta)$ is calculated as a function of centrality and associated particle momentum by mixed events using a trigger jet from an EMCal-triggered event and associated hadrons from minimum bias events or semi-central triggered events. The mixed event procedure will also remove the trivial correlation due to an η dependence in the single particle and track distributions. However, since there is little η dependence in either tracks or jets within the acceptance used in this analysis, the dominant effect is the pair acceptance. Mixed events are constructed separately for 30–40% and 40–50% centrality classes. The mixed events are required to be within the same 10% centrality class and have vertex positions within 2 cm along the direction of the beam, z_{vtx} . There is no difference in the correction within uncertainties for different orientations of the jet relative to the event plane, and therefore the same correction $a(\Delta\phi, \Delta\eta)$ is applied for all angles relative to the event plane. All associated momentum bins for $p_T > 2.0$ GeV/ c are combined to increase statistics because $a(\Delta\phi, \Delta\eta)$ has little momentum dependence at high momenta. The correction $a(\Delta\phi, \Delta\eta)$ is normalized to one at its maximum with the systematic uncertainty in the normalization determined by using different regions in $\Delta\phi$ and $\Delta\eta$, with a systematic uncertainty below 0.5% for all p_T^{assoc} bins used in this analysis. There is an additional shape uncertainty due to slight changes in the correlation function at large $\Delta\eta$ in the acceptance with z_{vtx} position. Since the background level is determined from the level of the correlation function at large $\Delta\eta$, this leads to a scale uncertainty in the background subtraction. This uncertainty is determined by varying the binning of the mixed events in z_{vtx} and is correlated for different angles relative to the event plane and for different bins in p_T^{assoc} . This scale uncertainty is used later for determining a systematic uncertainty on the background subtraction and is dependent on p_T^{assoc} .

3.4 Background subtraction

The signal in equation 4 has a large combinatorial background from particles created by processes other than the hard process which created the jet. The jet signal may be correlated with the second order event plane because of jet quenching, and soft hadrons are correlated with the second order event plane due to hydrodynamical flow. The Fourier expansion of this background can be expressed by:

$$\frac{dN}{\pi d\Delta\phi} = B \left(1 + \sum_{n=1}^{\infty} 2\tilde{v}_n^{\text{trig}} \tilde{v}_n^{\text{assoc}} \cos(n\Delta\phi) \right), \quad (5)$$

where $\tilde{v}_n^{\text{trig}}$ and $\tilde{v}_n^{\text{assoc}}$ refer to the effective Fourier coefficients for the azimuthal anisotropy of the trigger jet and associated hadron, respectively, to the background. For inclusive measurements, if the background is dominantly due to flow, the \tilde{v}_n of this background will be equal to the v_n due to flow. The exact values may be slightly different due to differences in the event samples, varying sensitivity in the method to fluctuations in the v_n and non-flow, the difference between the average over all pairs $\langle \tilde{v}_n^{\text{trig}} \tilde{v}_n^{\text{assoc}} \rangle$ and the product of the averages over all events $\langle \tilde{v}_n^{\text{trig}} \rangle \langle \tilde{v}_n^{\text{assoc}} \rangle$, differences in the v_n for particles in jets and from the bulk, and decorrelations between symmetry planes for hard and soft processes.

The contribution from these soft processes is subtracted using the RPF method [27]. This method avoids contamination by the near- and away-side jets by focusing on the near-side only at large $\Delta\eta$ and instead using the dependence of the flow-modulated background on the angle of the trigger jet relative to the event plane to constrain the background shape and level. For in-plane jets, background particles are more likely to be near the trigger jet than π away in azimuth, leading to a higher $\cos(2\Delta\phi)$ term, and the background level is higher because there are more jets in-plane. For out-of-plane jets, background particles are less likely to be near the trigger jet, leading to a negative $\cos(2\Delta\phi)$ term, and the background is lower because there are fewer jets. Because the second and fourth order event planes are correlated, a similar argument holds for the fourth order terms. These effects help constrain the even n terms and help distinguish them from the odd n terms and constrain the background level while avoiding contamination from the near- and away-side jets.

The event plane dependence can be used to determine the background shape and level. When the angle of the jet is fixed relative to the event plane, the effective size and shape of the background is given by

$$\begin{aligned} \tilde{B} &= \frac{N_t N_a c}{\pi^2} \left(1 + 2 \sum_{k=1}^{\infty} \frac{v_{2k}^{\text{trig}}}{2kc} \sin(2kc) \Re_{2k} C_{2k,0} \cos(2k\phi_s) \right), \quad (6) \\ \tilde{v}_n^{\text{trig}} &= \frac{v_n + \frac{\delta_{n,\text{mult}} 2}{nc} \sin(nc) \Re_n C_{n,0} \cos(n\phi_s) + \sum_{k=1}^{\infty} (v_{2k+n}^{\text{trig}} C_{|2k+n|,n} + v_{|2k-n|}^{\text{trig}} C_{|2k-n|,n}) \frac{\sin(2kc) \cos(2k\phi_s) \Re_{2k}}{2kc}}{1 + 2 \sum_{k=1}^{\infty} \frac{v_{2k}^{\text{trig}}}{2kc} \sin(nc) \Re_{2k} C_{2k,0} \cos(2k\phi_s)} \\ C_{n,m} &= \langle \cos(n\psi_n + m\psi_m - (n+m)\psi_2) \rangle \end{aligned}$$

where ϕ_s is the center of the azimuthal range of the trigger particle relative to the event plane, c is the width of that range, N_t is the number of triggers, N_a is the number of associated particles, v_n^{assoc} are the v_n of the associated particles, v_n^{trig} are the v_n of the triggers, and \Re_n is the event plane resolution given in equation 3 [66, 67]. Terms v_n with $n < 1$ are zero. The $C_{n,m}$ terms are a measure of how correlated event planes of different orders are with the second order event plane and are approximately zero when either n or m is odd. This is consistent with the weak correlation between the $n = 2$ participant plane and odd order participant planes [68] because the odd \tilde{v}_n arise mainly due to fluctuations in the initial state. In this case, the even \tilde{v}_n will change when the angle of the jet relative to the event plane is changed while the odd

\tilde{v}_n remain constant. The equation is expanded to include terms up to v_4 . The term $C_{2,0} = 1$ and the terms $C_{4,0}$ and $C_{4,2}$ are approximated to be one. The latter assumption will lead to an inconsistency between the v_4 from independent measurements and from the fit, but the fit will still provide a valid description of the background.

The shape of the background depends on the \mathfrak{R}_n , which are fixed at the measured values. The fourth order event plane resolution is calculated relative to the second order event plane, consistent with the shape described in equation 6. The uncertainties on the event plane resolution are negligible relative to the statistical and background fit uncertainties of the final results.

The jet signal in equation 4 can be decomposed into a near-side and an away-side. The near-side is a peak which is narrow in both $\Delta\phi$ and $\Delta\eta$, meaning that it is negligible at large $\Delta\eta$, while the away-side is narrow in $\Delta\phi$ but broad in $\Delta\eta$. The correlation function at large $\Delta\eta$ ($0.8 < |\Delta\eta| < 1.2$) and small $\Delta\phi$ ($|\Delta\phi| < \pi/2$) is fit simultaneously for \tilde{v}_n up to $n = 4$ for trigger jets in-plane ($|\psi - \phi_{jet}| < \pi/6$), mid-plane ($\pi/6 < |\psi - \phi_{jet}| < \pi/3$), and out-of-plane ($|\psi - \phi_{jet}| > \pi/3$), shown in fig. 1, to determine the background shape and level. Because the even \tilde{v}_n depend on the angle of the jet relative to the event plane, as shown in equation 6, the \tilde{v}_2 and \tilde{v}_4 of both the trigger jet and the associated particle are determined in the fit while only the product $\tilde{v}_3^{jet} \tilde{v}_3^{assoc}$ is extracted from the fit. A rapidity-even \tilde{v}_1 term can arise due to both momentum conservation and fluctuations in the initial state. This rapidity-even \tilde{v}_1 has been measured for single hadrons and is comparable in magnitude to \tilde{v}_2 and \tilde{v}_3 [69, 70]. This term does not change when the angle of the trigger jet is varied relative to the event plane so the product $\tilde{v}_1^{jet} \tilde{v}_1^{assoc}$ contributes to the background. When the fit function is varied to include this $n = 1$ term, it is zero within uncertainties and did not lead to significant differences in the correlation function. Since \tilde{v}_1^{assoc} is known to be non-zero, this likely means that \tilde{v}_1^{jet} is near zero. For associated particles above $p_T > 2$ GeV/c, the background is low and the statistics for the region which is background-dominated on the near-side are therefore also low, so the fit is restricted up to $n = 3$. The fits used in this analysis therefore have six parameters below 2 GeV/c, B , \tilde{v}_2^{jet} , \tilde{v}_2^{assoc} , $\tilde{v}_3^{jet} \tilde{v}_3^{assoc}$, \tilde{v}_4^{jet} , and \tilde{v}_4^{assoc} , and four above. The event plane resolution is fixed and variations within the uncertainties lead to negligible differences in the correlation functions.

Figure 3 shows a sample correlation function in the region which is background-dominated on the near-side compared to the fit for in-plane (a), mid-plane (b), and out-of-plane (c) jets and all jets combined (d) for associated particles with momenta $1.5 < p_T^{assoc} < 2.0$ GeV/c. Correlation functions for other p_T^{assoc} ranges used in this analysis are given in [71]. The ratio of the difference between the data and the fit to the fit is shown in fig. 3(e-h), showing that the fit describes the data well. The background subtracted correlation functions in the region $|\Delta\eta| < 0.6$ are shown in fig. 3(i-l). The uncertainties from the background subtraction are propagated using the covariance matrix from the fit. These uncertainties are non-trivially correlated point-to-point and between different bins relative to the event plane and are shown as a blue band. The scale uncertainties on the background are shown as a green band and are correlated point-to-point and between different bins relative to the event plane. The uncertainties due to the single track reconstruction efficiency, contamination, and the normalization of the acceptance correction are uncorrelated with each other but correlated for all points. These uncertainties are combined and listed as the scale uncertainty. The \tilde{v}_2^{jet} and \tilde{v}_2^{assoc} extracted from the fits are in agreement with other ALICE results [30, 33].

Finite event plane resolution reduces the event plane dependence of the signal because the measurement in one bin relative to the event plane will have contributions from other bins as well. Techniques for correcting for this effect increase the event plane dependence observed in the uncorrected data [72], but if there is no event plane dependence in the uncorrected data, these corrections will not reveal an event plane dependence. Since no event plane dependence is observed within uncertainties and corrections would increase the complexity of the measurement and the systematic uncertainties, no correction is applied for the finite event plane resolution. The impact of the finite event plane resolution is discussed

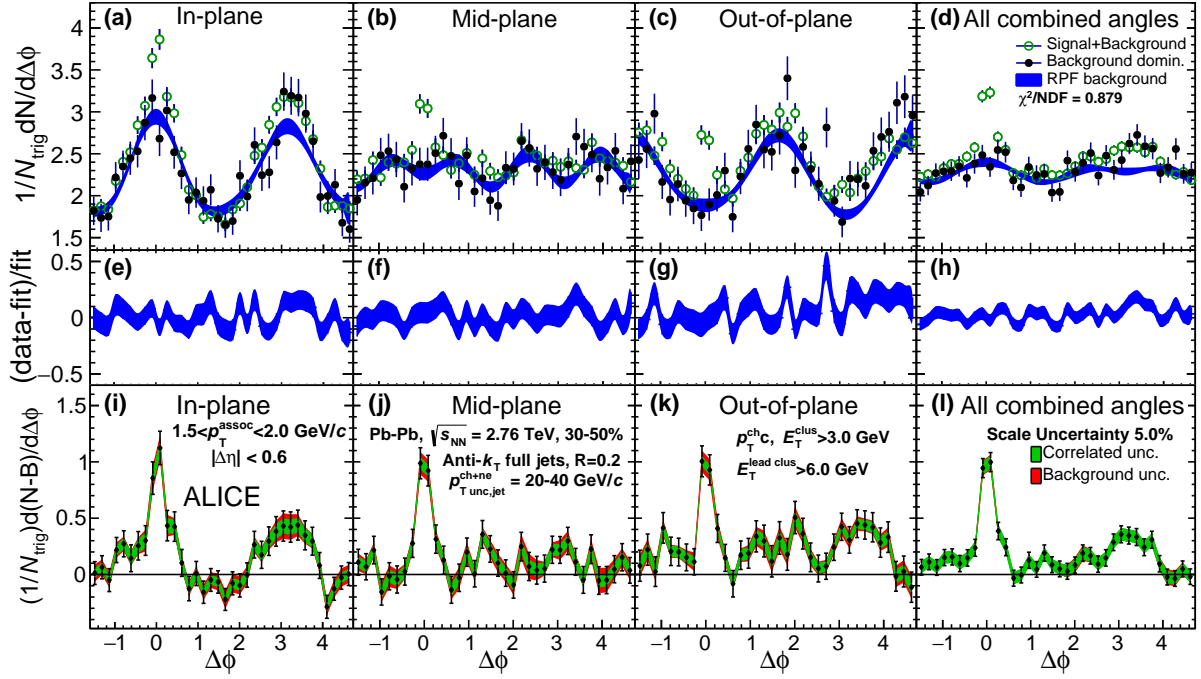


Figure 3: The signal plus background region, $|\Delta\eta| < 0.6$ (green points), the region which is background-dominated on the near-side, $0.8 < |\Delta\eta| < 1.2$ (black points), and the RPF fit to $|\Delta\phi| < \pi/2$ (blue band) to the region which is background-dominated on the near-side for $20 < p_T^{\text{jet}} < 40$ GeV/c jets correlated with $1.5 < p_T^{\text{assoc}} < 2.0$ GeV/c hadrons from 30-50% centrality collisions on the top panel. The middle panel shows the quality of the RPF fit to the region which is background-dominated on the near-side, $(\text{data}-\text{fit})/\text{fit}$. On the bottom panel are the RPF corrected correlation functions, with the uncertainty from the background fit (red band), and the correlated uncertainty (green band).

in sec. 3.6.

3.5 Associated track yields and peak widths

The yield of tracks associated with jets is calculated by integrating the associated yield:

$$Y = \frac{1}{N_{\text{trig}}} \int_{\eta_1}^{\eta_2} \int_{\phi_1}^{\phi_2} \frac{d(N_{\text{meas}} - N_{\text{bkgd}})}{d\Delta\phi} d\Delta\phi d\Delta\eta. \quad (7)$$

The integration limits of $\phi_1 = -\pi/3$ and $\phi_2 = \pi/3$ for the near-side, $\phi_1 = 2\pi/3$ and $\phi_2 = 4\pi/3$ for the away-side, and $\eta_1 = -0.6$ and $\eta_2 = 0.6$ for both are part of the definition of the measurement. The systematic uncertainties due to the extraction of the background from the RPF are propagated using the covariance matrix from the fit. This uncertainty is non-trivially correlated between yields for different angles of the jet relative to the event plane and for the near- and away-side and uncorrelated for points at different $p_{\text{T}}^{\text{assoc}}$. The shape uncertainty in the acceptance correction at large $\Delta\eta$ leads to an additional scale uncertainty when propagating the background determined in the region $0.8 < |\Delta\eta| < 1.2$ to the region ($|\Delta\eta| < 0.6$). This uncertainty is 100% correlated for all data points. The single track reconstruction efficiency uncertainty, the uncertainty due to normalization of the acceptance correction, and the uncertainty due to contamination from secondary particles are 100% correlated for all points and affect the scale of the correlation functions and the yields.

The ratios and differences of yields are calculated in order to investigate possible event plane dependent modifications. The systematic uncertainties from the background largely cancel out in the ratio and the difference. The track reconstruction efficiency, mixed event normalization, and secondary contamination systematic uncertainties cancel out in the ratio.

The widths are quantified by fitting the correlation functions to a Gaussian, $Ae^{(\Delta\phi - \Delta\phi_0)^2/2\sigma^2}$ where $\Delta\phi_0 = 0$ on the near-side and $\Delta\phi_0 = \pi$ on the away-side, in the range $|\Delta\phi| < \pi/3$ on the near-side and $|\Delta\phi - \pi| < \pi/3$ on the away-side. The near- and away-side are fit separately. The Gaussian fit is repeated with different values of the background parameters and the covariance matrix is used to propagate the uncertainties.

The systematic uncertainties are summarized in tab. 1 and tab. 2. Table 1 lists the sources of systematic uncertainties which are independent of the angle relative to the event plane and the momentum, including the single track reconstruction efficiency (sec. 2), contamination from secondaries (sec. 2), uncertainties in the mixed events due to their normalization and shape in $\Delta\phi$ (sec. 3.3), and uncertainties in the event plane resolution (sec. 3.2). The uncertainties in the single track reconstruction efficiency, normalization of the acceptance correction determined from mixed events, and secondary contamination lead to a 5% uncertainty in the scale of the correlation functions and yields. This uncertainty is uncorrelated for different associated particle momenta.

Table 2 lists uncertainties which are dependent on the angle of the jet relative to the event plane and the associated particle's momentum on the yields due to the scale uncertainty in the mixed events (sec. 3.3) and in the background fit (sec. 3.4) for a few representative associated particle momenta. The uncertainty of the acceptance correction determined from mixed events in $\Delta\eta$ and the uncertainty due to the background subtraction are different for different $p_{\text{T}}^{\text{assoc}}$ bins and therefore shown separately for each data point. The uncertainty due to the shape uncertainty of the acceptance correction determined from mixed events in $\Delta\eta$ is correlated for different angles relative to the event plane and uncorrelated between different $p_{\text{T}}^{\text{assoc}}$ bins. The uncertainty due to the background subtraction is non-trivially correlated for different angles of the jet relative to the event plane but uncorrelated between different $p_{\text{T}}^{\text{assoc}}$ bins.

Table 1: Summary of systematic uncertainties which are independent of the angle relative to the event plane and the momentum for $20 < p_T^{\text{jet}} < 40$ GeV/c in 30-50% central Pb–Pb collisions.

Source	Uncertainty %
Single particle reconstruction efficiency	4
Contamination	1
Mixed event (shape $\Delta\phi$)	negligible
Mixed event normalization	< 0.5
event plane resolution	negligible

Table 2: Summary of systematic uncertainties on the yields and widths calculated from the correlation functions due to the shape uncertainty coming from the shape of the acceptance correction in $\Delta\eta$ and the correlated background fit uncertainty, both varying with event plane orientation bins. They are displayed for $20 < p_T^{\text{jet}} < 40$ GeV/c in 30-50% central Pb–Pb collisions for $1.0 < p_T^{\text{assoc}} < 1.5$ GeV/c and $3.0 < p_T^{\text{assoc}} < 4.0$ GeV/c bins. The values are expressed as a percent of the nominal value.

Source	Result	Orientation	Uncertainty %			
			Near-side: p_T^{assoc} (GeV/c)		Away-side: p_T^{assoc} (GeV/c)	
			1.0-1.5	3.0-4.0	1.0-1.5	3.0-4.0
Acceptance shape	Yield	in-plane	20	2.8	33	7.9
		mid-plane	13	2.7	25	9.2
		out-of-plane	10	2.5	22	6.3
	Width	in-plane	14	1.5	-	5.0
		mid-plane	9.8	1.4	-	7.1
		out-of-plane	5.9	0.9	-	4.6
Background fit	Yield	in-plane	16	6.3	50	18
		mid-plane	9.3	3.9	37	13
		out-of-plane	7.9	6.0	35	15
	Width	in-plane	23	4.2	-	12
		mid-plane	25	2.7	-	23
		out-of-plane	10	3.0	-	11

3.6 Impact of event plane resolution

To understand the impact of a possible event plane dependence in the signal, we consider the Fourier decomposition approach to correcting for the event plane resolution as in [72]. We can quantify the true azimuthal anisotropy of the signal by a Fourier decomposition as

$$S(\Delta\phi)\left(1 + 2 \sum_{n=1}^{\infty} v_n^{\text{quench}} \cos(\phi^{\text{trig}} - \psi)\right), \quad (8)$$

where $S(\Delta\phi)$ is the correlation function of the signal averaged over all angles relative to the event plane, the v_n^{quench} are due to jet quenching, and ϕ^{trig} is the azimuthal angle of the trigger particle. The v_n^{quench} could also be a function of $\Delta\phi$. The measured azimuthal anisotropy of the signal is then given by

$$S\left(1 + 2 \sum_{n=1}^{\infty} \mathfrak{R}_n v_n^{\text{quench}} \cos(\phi^{\text{trig}} - \psi)\right). \quad (9)$$

Note that the v_n^{quench} are distinct from both the v_n from flow and the jet v_n . The jet v_n measured in [33, 34] are anisotropies in the number of jets relative to the event plane while the v_n^{quench} are a measure of the anisotropies of the constituents of those jets. Precision extraction of the v_n^{quench} would require measurements of the signal in several bins of $\phi^{\text{trig}} - \psi$ and is not feasible for this measurement. Equation 9 shows that the impact of the finite event plane resolution is small, since for this analysis $\mathfrak{R}_2 = 0.73$.

If we assume that the v_n^{quench} do not depend on $\Delta\phi$, the yields are given by integrating the equation 9 over the same angles of the trigger particle relative to the event plane. The in-plane (Y_{IP}), mid-plane (Y_{MP}), and out-of-plane (Y_{OP}) yields up to $n = 3$ in terms of the average yield (Y) are then given by

$$\begin{aligned} Y_{\text{IP}} &= Y\left(1 + \frac{6}{\pi} \mathfrak{R}_1 v_1^{\text{quench}} + \frac{3\sqrt{3}}{\pi} \mathfrak{R}_2 v_2^{\text{quench}} + \frac{4}{\pi} \mathfrak{R}_3 v_3^{\text{quench}}\right) \\ Y_{\text{MP}} &= Y\left(1 + \frac{6(\sqrt{3}-1)}{\pi} \mathfrak{R}_1 v_1^{\text{quench}} - \frac{4}{\pi} \mathfrak{R}_3 v_3^{\text{quench}}\right) \\ Y_{\text{OP}} &= Y\left(1 - \frac{3\sqrt{3}}{\pi} \mathfrak{R}_2 v_2^{\text{quench}}\right). \end{aligned} \quad (10)$$

The differences and ratios of the yields up to $n = 3$ are then

$$\begin{aligned} \frac{Y_{\text{OP}}}{Y_{\text{IP}}} &\approx \frac{Y_{\text{OP}} - Y_{\text{IP}}}{Y} \approx 1 - \frac{6}{\pi} \mathfrak{R}_1 v_1^{\text{quench}} - \frac{6\sqrt{3}}{\pi} \mathfrak{R}_2 v_2^{\text{quench}} - \frac{4}{\pi} \mathfrak{R}_3 v_3^{\text{quench}} \\ \frac{Y_{\text{MP}}}{Y_{\text{IP}}} &\approx \frac{Y_{\text{MP}} - Y_{\text{IP}}}{Y} \approx 1 - \frac{6\sqrt{3}-12}{\pi} \mathfrak{R}_1 v_1^{\text{quench}} - \frac{3\sqrt{3}}{\pi} \mathfrak{R}_2 v_2^{\text{quench}} - \frac{8}{\pi} \mathfrak{R}_3 v_3^{\text{quench}}. \end{aligned} \quad (11)$$

Since the coefficients of the v_n^{quench} are on the order of one, the deviations of these ratios from one are on the order of the v_n^{quench} . The odd v_n^{quench} will partially cancel out because they will have opposite signs on different sides of the event plane and in the absence of surface bias, they will cancel out completely. The $n = 2$ term is therefore likely the dominant term. We use this expression to evaluate the approximate effect of the event plane resolution. The allowed range of v_n^{quench} is $-0.5 < v_2^{\text{quench}} < 0.5$, with positive (negative) values indicating suppression (enhancement) of the constituents. While the v_n^{quench} is a measure of the asymmetry of modifications of jets relative to the event plane rather than the distribution of jets,

we consider the asymmetry in the number of jets [33, 34], $v_2^{\text{jet}} = 0.1$, as a reasonable value of v_n^{quench} . This would lead to $\frac{Y_{\text{OP}}}{Y_{\text{IP}}} \approx \frac{Y_{\text{OP}} - Y_{\text{IP}}}{Y} \approx 0.67$ and $\frac{Y_{\text{MP}}}{Y_{\text{IP}}} \approx \frac{Y_{\text{MP}} - Y_{\text{IP}}}{Y} \approx 0.83$ with perfect event plane resolution ($\mathfrak{R}_2 = 1.0$) and $\frac{Y_{\text{OP}}}{Y_{\text{IP}}} \approx \frac{Y_{\text{OP}} - Y_{\text{IP}}}{Y} \approx 0.75$ and $\frac{Y_{\text{MP}}}{Y_{\text{IP}}} \approx \frac{Y_{\text{MP}} - Y_{\text{IP}}}{Y} \approx 0.88$ with the event plane resolution in this analysis, $\mathfrak{R}_2 = 0.73$.

4 Results

The near-side and away-side jet yields as a function of $p_{\text{T}}^{\text{assoc}}$ for $20 < p_{\text{T}}^{\text{jet}} < 40$ GeV/c full jets in 30-50% central Pb–Pb collisions are shown in fig. 4 for jets reconstructed in-plane, mid-plane, and out-of-plane for $1.0 < p_{\text{T}}^{\text{assoc}} < 1.5$ GeV/c, $1.5 < p_{\text{T}}^{\text{assoc}} < 2.0$ GeV/c, $2.0 < p_{\text{T}}^{\text{assoc}} < 3.0$ GeV/c, $3.0 < p_{\text{T}}^{\text{assoc}} < 4.0$ GeV/c, $4.0 < p_{\text{T}}^{\text{assoc}} < 5.0$ GeV/c, $5.0 < p_{\text{T}}^{\text{assoc}} < 6.0$ GeV/c, and $6.0 < p_{\text{T}}^{\text{assoc}} < 10.0$ GeV/c. The dominant feature is the decrease in the yield with increasing $p_{\text{T}}^{\text{assoc}}$. Note that yields with $p_{\text{T}}^{\text{assoc}} > 3$ GeV/c include jet constituents, complicating the interpretation of these data points. We therefore focus on lower momentum on the near-side and on the away-side.

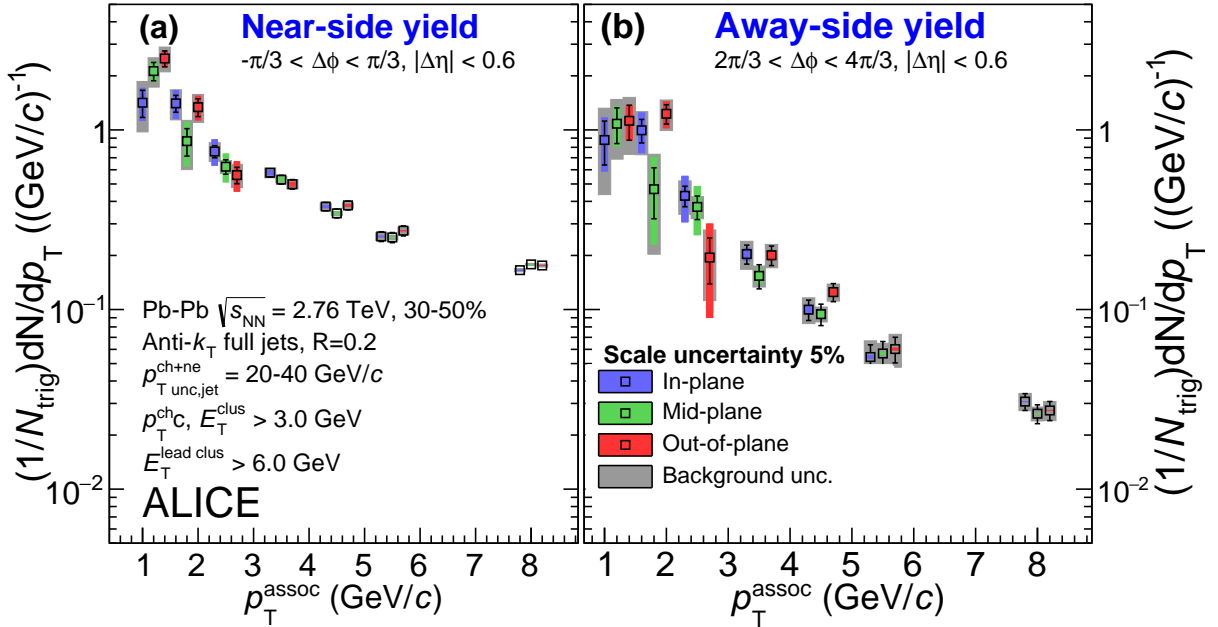


Figure 4: The (a) near-side and (b) away-side yield vs $p_{\text{T}}^{\text{assoc}}$ for $20 < p_{\text{T}}^{\text{jet}} < 40$ GeV/c full jets of 30-50% centrality in Pb–Pb collisions. The gray band corresponds to the background uncertainty, which is non-trivially correlated point-to-point [27, 37]. The colored bands are the systematic uncertainties coming from the shape uncertainty of the acceptance correction. There is an additional 5% global scale uncertainty. Points are displaced for visibility.

Jet-hadron correlations can be used to measure changes in the momentum balance within the jet, as in [24]. Partonic energy loss will shift energy in the jet from higher momentum constituents to lower momentum constituents, so if jets in-plane interact less with the medium, the differences $Y_{\text{mid}} - Y_{\text{in}}$ and $Y_{\text{out}} - Y_{\text{in}}$ will be negative at high momenta and positive at low momenta. For these differences, the systematic uncertainties partially cancel out. Figure 5 shows the yield differences $Y_{\text{mid}} - Y_{\text{in}}$ and $Y_{\text{out}} - Y_{\text{in}}$ for the near- and away-side. There is no event plane dependence within uncertainties, consistent with expectations if $v_2^{\text{quench}} \approx 0.1$ as observed for inclusive jet production. Comparisons between yields in jet-hadron correlations in Au–Au and pp collisions demonstrated suppression at high momenta and an enhancement at low momenta in Au–Au collisions at $\sqrt{s_{\text{NN}}} = 200$ GeV [24]. The lack of an event plane

dependence therefore indicates that any dependence of these modifications on the average path length is less than our experimental uncertainties.

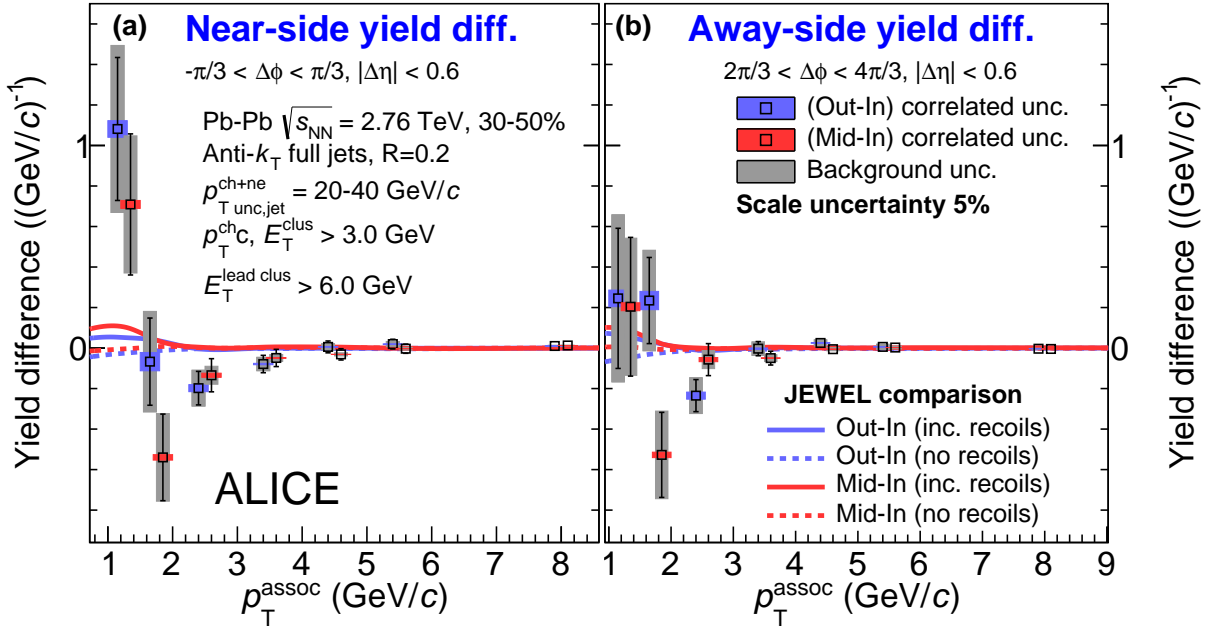


Figure 5: The (a) near-side and (b) away-side yield differences vs p_T^{assoc} for $20 < p_T^{\text{jet}} < 40$ GeV/c full jets of 30-50% centrality in Pb–Pb collisions. The gray band corresponds to the background uncertainty, which is non-trivially correlated point-to-point [27, 37]. The colored bands are the systematic uncertainties coming from the shape uncertainty of the acceptance correction. There is an additional 5% global scale uncertainty. Points are displaced for visibility.

To better quantify and examine the event plane dependence of the yields, ratios of mid-plane yields relative to in-plane yields $Y_{\text{mid}}/Y_{\text{in}}$ and out-of-plane yields relative to in-plane yields $Y_{\text{out}}/Y_{\text{in}}$ as a function of p_T^{assoc} are shown in fig. 6 for both the near- and away-sides. As for the yield differences, a substantial fraction of the systematic uncertainties cancel out for the ratios. If medium modifications increase with increasing path length traversed by the parton, these ratios will be less than one at high momenta and greater than one at low momenta. These ratios are consistent with one for all p_T^{assoc} . In contrast, R_{AA} can be as low as 0.1 [7], indicating partonic energy loss.

The modification of the correlated yield ratios $Y_{\text{mid}}/Y_{\text{in}}$ and $Y_{\text{out}}/Y_{\text{in}}$ due to jet quenching can be estimated from equation 11 as approximately $3.3 \times \mathfrak{R}_2 v_2^{\text{quench}}$ for out-of-plane to in-plane ratios and $1.7 \times \mathfrak{R}_2 v_2^{\text{quench}}$ for mid-plane to in-plane ratios following the logic in sec. 3.6. Since $\mathfrak{R}_2 = 0.73$, the ratios in fig. 6 can be used to constrain a hypothetical v_2^{quench} . While v_2^{quench} is a measure of the azimuthal asymmetry in jet modifications rather than the number of jets, we use the asymmetry in the number of jets, $v_2^{\text{jet}} = 0.1$ [33, 34], as a reasonable value for v_2^{quench} . If $v_2^{\text{quench}} = 0.1$, the out-of-plane to in-plane ratios would be 0.75 and the mid-plane to in-plane ratios would be 0.88. The data in fig. 6 are therefore consistent both with v_2^{quench} comparable to the inclusive jet asymmetry and with no asymmetry.

To investigate whether or not there is a systematic change in the ratio of yields with the angle of the jet relative to the event plane, we fit the data in fig. 6 to a constant. The systematic uncertainties are treated as uncorrelated point-to-point and added in quadrature to the statistical uncertainties. The results are given in tab. 3 and are consistent with yield ratios of one. We note that medium modifications could result in a p_T^{assoc} dependence and this could be exacerbated by kinematic biases on the near side because

Table 3: Results of fits to fig. 6 to a constant c , the χ^2 over the number of degrees of freedom (NDF), the number of standard deviations σ of c from one, and the range of c within a 90% confidence limit (CL).

parameter	Near-side		Away-side	
	$Y_{\text{out}}/Y_{\text{in}}$	$Y_{\text{mid}}/Y_{\text{in}}$	$Y_{\text{out}}/Y_{\text{in}}$	$Y_{\text{mid}}/Y_{\text{in}}$
c	0.972 ± 0.037	0.960 ± 0.036	0.885 ± 0.079	0.835 ± 0.078
χ^2/NDF	2.5	2.4	2.4	0.8
σ	-0.8	-1.1	-1.5	-2.1
90% CL	0.91 – 1.03	0.90 – 1.02	0.75 – 1.02	0.71 – 0.96

associated particles with momenta above 3 GeV/ c are included in jet reconstruction. The χ^2 per degree of freedom may be large either because this procedure averages over different physical effects which change with momentum or because of point-to-point correlations in the uncertainties.

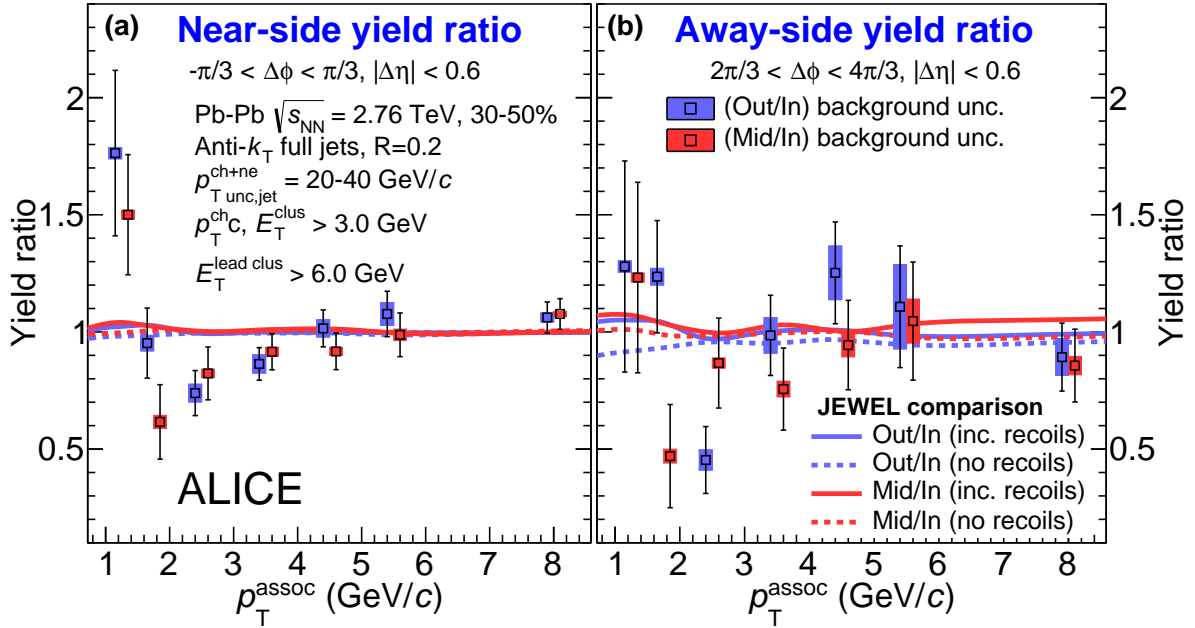


Figure 6: The (a) near-side and (b) away-side yield ratios vs p_T^{assoc} for $20 < p_T^{\text{jet}} < 40$ GeV/ c full jets of 30-50% centrality in Pb–Pb collisions. The colored bands correspond to the background uncertainty, which is non-trivially correlated point-to-point [27, 37]. The systematic uncertainties coming from the shape uncertainty of the acceptance correction cancel out for the ratios. Points are displaced for visibility.

Figure 7 shows the widths from a fit to the Gaussian for the near- and away-side. Broadening would be expected from either collisional energy loss or gluon bremsstrahlung and path length dependent energy loss would lead to a greater width for jets out-of-plane than in-plane. No event plane dependence is observed within uncertainties, indicating that any effect is smaller than the precision of the data.

The data in fig. 5 and fig. 6 are compared to calculations from JEWEL, a jet energy loss model based on radiative and collisional energy loss in connection with partons sampled from a longitudinally expanding medium [73]. An important setting in the model is the choice of whether or not to keep the recoiled partons sampled from the medium in the simulation. With no recoils, the lost jet momentum vanishes from the entire system, while including the recoils conserves the jet’s overall momentum, but adds energy and background particles (from the medium) to the simulated dijet. We compare to JEWEL with both recoils off and recoils on. Results with recoils off are useful for modeling energy loss in the hard part of the jet. Results with recoils on show where the jet’s lost momentum goes. Any experimental analysis

would likely include some but not all of the recoil particles in JEWEL, as some proportion of the recoil particles are indistinguishable from background.

JEWEL only predicts a slight event plane dependence, despite the path length dependence of partonic energy loss, due to the dominant impact of jet-by-jet fluctuations in partonic energy loss over path length dependence [38, 74]. The slight event plane dependence predicted by JEWEL is well below the systematic uncertainty in the measurement. The agreement of JEWEL with the data is therefore consistent with path length dependence having an insignificant impact compared to jet-by-jet fluctuations in energy loss, although fluctuations in the density of the medium (not included in the JEWEL model) may also suppress observable path length dependence.

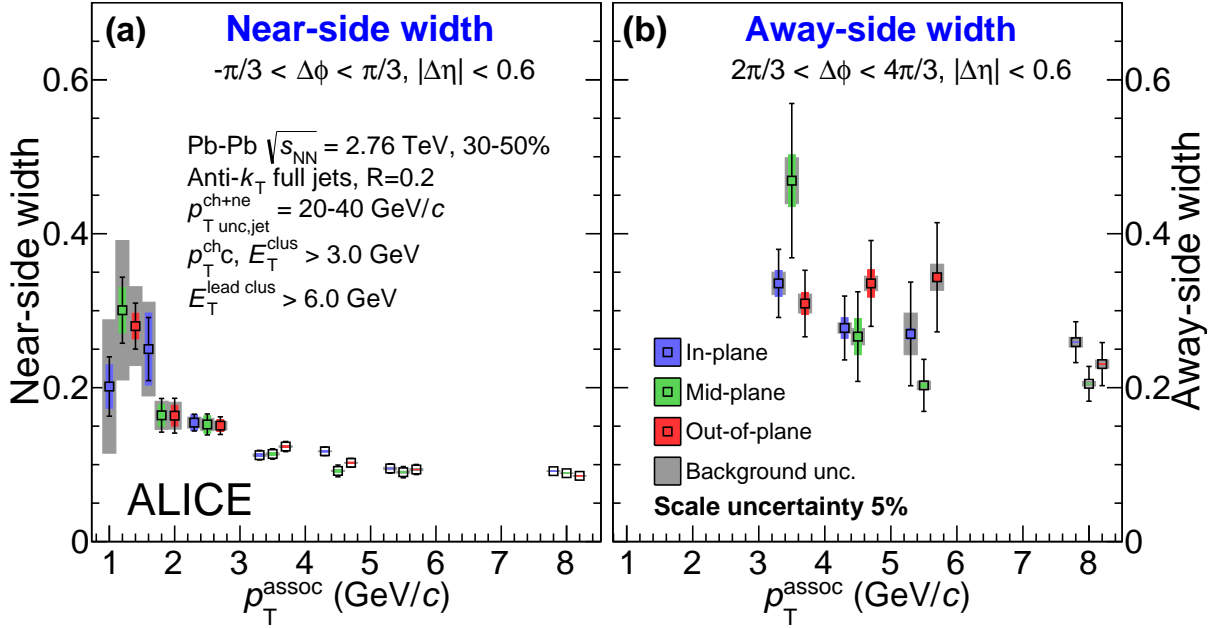


Figure 7: The (a) near-side and (b) away-side widths vs p_T^{assoc} for $20 < p_T^{\text{jet}} < 40$ GeV/c full jets of 30–50% centrality in Pb–Pb collisions. The gray band corresponds the background uncertainty, which is non-trivially correlated point-to-point [27, 37]. The colored bands are the systematic uncertainties coming from the shape uncertainty of the acceptance correction. Points are displaced for visibility.

5 Conclusions

Partonic interactions depend on the length traversed in the medium, so any medium modifications of the jet are expected to be path length dependent. The path length traversed by a jet is correlated on average with the angle of the jet with respect to the event plane. The use of the RPF method for background subtraction reduces the assumptions required for background subtraction and since the determination of the background is currently limited by statistics, it is likely that future studies could reduce these systematic uncertainties. Measurements of jet-hadron correlations relative to the event plane in Pb–Pb collisions at $\sqrt{s_{\text{NN}}} = 2.76$ TeV are presented. Results are consistent with no dependence in the yields or the widths on the angle of the jet relative to the event plane within uncertainties. This may indicate that jet-by-jet fluctuations in partonic energy loss are important for a full description of medium modifications of jets.

Acknowledgements

The ALICE Collaboration would like to thank all its engineers and technicians for their invaluable contributions to the construction of the experiment and the CERN accelerator teams for the outstanding performance of the LHC complex. The ALICE Collaboration gratefully acknowledges the resources and support provided by all Grid centres and the Worldwide LHC Computing Grid (WLCG) collaboration. The ALICE Collaboration acknowledges the following funding agencies for their support in building and running the ALICE detector: A. I. Alikhanyan National Science Laboratory (Yerevan Physics Institute) Foundation (ANSL), State Committee of Science and World Federation of Scientists (WFS), Armenia; Austrian Academy of Sciences, Austrian Science Fund (FWF): [M 2467-N36] and Nationalstiftung für Forschung, Technologie und Entwicklung, Austria; Ministry of Communications and High Technologies, National Nuclear Research Center, Azerbaijan; Conselho Nacional de Desenvolvimento Científico e Tecnológico (CNPq), Financiadora de Estudos e Projetos (Finep), Fundação de Amparo à Pesquisa do Estado de São Paulo (FAPESP) and Universidade Federal do Rio Grande do Sul (UFRGS), Brazil; Ministry of Education of China (MOEC) , Ministry of Science & Technology of China (MSTC) and National Natural Science Foundation of China (NSFC), China; Ministry of Science and Education and Croatian Science Foundation, Croatia; Centro de Aplicaciones Tecnológicas y Desarrollo Nuclear (CEADEN), Cubaenergía, Cuba; Ministry of Education, Youth and Sports of the Czech Republic, Czech Republic; The Danish Council for Independent Research | Natural Sciences, the VILLUM FONDEN and Danish National Research Foundation (DNRF), Denmark; Helsinki Institute of Physics (HIP), Finland; Commissariat à l’Energie Atomique (CEA), Institut National de Physique Nucléaire et de Physique des Particules (IN2P3) and Centre National de la Recherche Scientifique (CNRS) and Région des Pays de la Loire, France; Bundesministerium für Bildung und Forschung (BMBF) and GSI Helmholtzzentrum für Schwerionenforschung GmbH, Germany; General Secretariat for Research and Technology, Ministry of Education, Research and Religions, Greece; National Research, Development and Innovation Office, Hungary; Department of Atomic Energy Government of India (DAE), Department of Science and Technology, Government of India (DST), University Grants Commission, Government of India (UGC) and Council of Scientific and Industrial Research (CSIR), India; Indonesian Institute of Science, Indonesia; Centro Fermi - Museo Storico della Fisica e Centro Studi e Ricerche Enrico Fermi and Istituto Nazionale di Fisica Nucleare (INFN), Italy; Institute for Innovative Science and Technology , Nagasaki Institute of Applied Science (IIST), Japanese Ministry of Education, Culture, Sports, Science and Technology (MEXT) and Japan Society for the Promotion of Science (JSPS) KAKENHI, Japan; Consejo Nacional de Ciencia (CONACYT) y Tecnología, through Fondo de Cooperación Internacional en Ciencia y Tecnología (FONCICYT) and Dirección General de Asuntos del Personal Académico (DGAPA), Mexico; Nederlandse Organisatie voor Wetenschappelijk Onderzoek (NWO), Netherlands; The Research Council of Norway, Norway; Commission on Science and Technology for Sustainable Development in the South (COMSATS), Pakistan; Pontificia Universidad Católica del Perú, Peru; Ministry of Science and Higher Education and National Science Centre, Poland; Korea Institute of Science and Technology Information and National Research Foundation of Korea (NRF), Republic of Korea; Ministry of Education and Scientific Research, Institute of Atomic Physics and Ministry of Research and Innovation and Institute of Atomic Physics, Romania; Joint Institute for Nuclear Research (JINR), Ministry of Education and Science of the Russian Federation, National Research Centre Kurchatov Institute, Russian Science Foundation and Russian Foundation for Basic Research, Russia; Ministry of Education, Science, Research and Sport of the Slovak Republic, Slovakia; National Research Foundation of South Africa, South Africa; Swedish Research Council (VR) and Knut & Alice Wallenberg Foundation (KAW), Sweden; European Organization for Nuclear Research, Switzerland; Suranaree University of Technology (SUT), National Science and Technology Development Agency (NSDTA) and Office of the Higher Education Commission under NRU project of Thailand, Thailand; Turkish Atomic Energy Agency (TAEK), Turkey; National Academy of Sciences of Ukraine, Ukraine; Science and Technology Facilities Council (STFC), United Kingdom; National Science Foundation of the United States of America (NSF) and United States

Department of Energy, Office of Nuclear Physics (DOE NP), United States of America.

References

- [1] **PHENIX** Collaboration, K. Adcox *et al.*, “Formation of dense partonic matter in relativistic nucleus-nucleus collisions at RHIC: Experimental evaluation by the PHENIX collaboration”, *Nucl. Phys.* **A757** (2005) 184–283, arXiv:nucl-ex/0410003 [nucl-ex].
- [2] **STAR** Collaboration, J. Adams *et al.*, “Experimental and theoretical challenges in the search for the quark gluon plasma: The STAR collaboration’s critical assessment of the evidence from RHIC collisions”, *Nucl. Phys.* **A757** (2005) 102–183, arXiv:nucl-ex/0501009.
- [3] **PHOBOS** Collaboration, B. B. Back *et al.*, “The PHOBOS perspective on discoveries at RHIC”, *Nucl. Phys.* **A757** (2005) 28–101, arXiv:nucl-ex/0410022.
- [4] **BRAHMS** Collaboration, I. Arsene *et al.*, “Quark Gluon Plasma and Color Glass Condensate at RHIC? The perspective from the BRAHMS experiment”, *Nucl. Phys.* **A757** (2005) 1–27, arXiv:nucl-ex/0410020.
- [5] **ALICE** Collaboration, K. Aamodt *et al.*, “Two-pion Bose-Einstein correlations in central Pb-Pb collisions at $\sqrt{s_{NN}} = 2.76$ TeV”, *Phys. Lett.* **B696** (2011) 328–337, arXiv:1012.4035 [nucl-ex].
- [6] **ALICE** Collaboration, K. Aamodt *et al.*, “Centrality dependence of the charged-particle multiplicity density at mid-rapidity in Pb-Pb collisions at $\sqrt{s_{NN}} = 2.76$ ”, *Phys. Rev. Lett.* **106** (2011) 032301, arXiv:1012.1657 [nucl-ex].
- [7] **ALICE** Collaboration, K. Aamodt *et al.*, “Suppression of Charged Particle Production at Large Transverse Momentum in Central Pb-Pb Collisions at $\sqrt{s_{NN}} = 2.76$ TeV”, *Phys. Lett.* **B696** (2011) 30–39, arXiv:1012.1004 [nucl-ex].
- [8] **ALICE** Collaboration, K. Aamodt *et al.*, “Charged-particle multiplicity density at mid-rapidity in central Pb-Pb collisions at $\sqrt{s_{NN}} = 2.76$ TeV”, *Phys. Rev. Lett.* **105** (2010) 252301, arXiv:1011.3916 [nucl-ex].
- [9] **ALICE** Collaboration, K. Aamodt *et al.*, “Elliptic flow of charged particles in Pb-Pb collisions at 2.76 TeV”, *Phys. Rev. Lett.* **105** (2010) 252302, arXiv:1011.3914 [nucl-ex].
- [10] **ATLAS** Collaboration, G. Aad *et al.*, “Observation of a Centrality-Dependent Dijet Asymmetry in Lead-Lead Collisions at $\sqrt{s_{NN}} = 2.76$ TeV with the ATLAS Detector at the LHC”, *Phys. Rev. Lett.* **105** (2010) 252303, arXiv:1011.6182 [hep-ex].
- [11] **CMS** Collaboration, S. Chatrchyan *et al.*, “Observation and studies of jet quenching in PbPb collisions at nucleon-nucleon center-of-mass energy = 2.76 TeV”, *Phys. Rev.* **C84** (2011) 024906, arXiv:1102.1957 [nucl-ex].
- [12] M. Connors, C. Nattrass, R. Reed, and S. Salur, “Jet measurements in heavy ion physics”, *Rev. Mod. Phys.* **90** (2018) 025005, arXiv:1705.01974 [nucl-ex].
- [13] G.-Y. Qin and X.-N. Wang, “Jet quenching in high-energy heavy-ion collisions”, *Int. J. Mod. Phys.* **E24** no. 11, (2015) 1530014, arXiv:1511.00790 [hep-ph]. [,309(2016)].
- [14] **STAR** Collaboration, J. Adams *et al.*, “Transverse momentum and collision energy dependence of high p(T) hadron suppression in Au+Au collisions at ultrarelativistic energies”, *Phys.Rev.Lett.* **91** (2003) 172302, arXiv:nucl-ex/0305015 [nucl-ex].

- [15] **PHENIX** Collaboration, S. Adler *et al.*, “Suppressed π^0 production at large transverse momentum in central Au+ Au collisions at $\sqrt{s_{NN}} = 200$ GeV”, *Phys.Rev.Lett.* **91** (2003) 072301, arXiv:nucl-ex/0304022 [nucl-ex].
- [16] **PHOBOS** Collaboration, B. Back *et al.*, “Pseudorapidity dependence of charged hadron transverse momentum spectra in d+Au collisions at $\sqrt{s_{NN}} = 200$ GeV”, *Phys.Rev.* **C70** (2004) 061901, arXiv:nucl-ex/0406017 [nucl-ex].
- [17] **CMS** Collaboration, S. Chatrchyan *et al.*, “Study of high-pT charged particle suppression in PbPb compared to pp collisions at $\sqrt{s_{NN}} = 2.76$ TeV”, *Eur.Phys.J.* **C72** (2012) 1945, arXiv:1202.2554 [nucl-ex].
- [18] **JET** Collaboration, K. M. Burke *et al.*, “Extracting the jet transport coefficient from jet quenching in high-energy heavy-ion collisions”, *Phys. Rev.* **C90** no. 1, (2014) 014909, arXiv:1312.5003 [nucl-th].
- [19] **ATLAS** Collaboration, G. Aad *et al.*, “Measurement of inclusive jet charged-particle fragmentation functions in Pb+Pb collisions at $\sqrt{s_{NN}} = 2.76$ TeV with the ATLAS detector”, *Phys.Lett.* **B739** (2014) 320–342, arXiv:1406.2979 [hep-ex].
- [20] **CMS** Collaboration, S. Chatrchyan *et al.*, “Measurement of jet fragmentation in PbPb and pp collisions at $\sqrt{s_{NN}} = 2.76$ TeV”, *Phys.Rev.* **C90** no. 2, (2014) 024908, arXiv:1406.0932 [nucl-ex].
- [21] **CMS** Collaboration, S. Chatrchyan *et al.*, “Measurement of jet fragmentation into charged particles in pp and PbPb collisions at $\sqrt{s_{NN}} = 2.76$ TeV”, *JHEP* **1210** (2012) 087, arXiv:1205.5872 [nucl-ex].
- [22] **PHENIX** Collaboration, A. Adare *et al.*, “Medium modification of jet fragmentation in Au + Au collisions at $\sqrt{s_{NN}} = 200$ GeV measured in direct photon-hadron correlations”, *Phys. Rev. Lett.* **111** no. 3, (2013) 032301, arXiv:1212.3323 [nucl-ex].
- [23] **STAR** Collaboration, G. Agakishiev *et al.*, “System size and energy dependence of near-side di-hadron correlations”, *Phys.Rev.* **C85** (2012) 014903, arXiv:1110.5800 [nucl-ex].
- [24] **STAR** Collaboration, L. Adamczyk *et al.*, “Jet-Hadron Correlations in $\sqrt{s_{NN}} = 200$ GeV $p + p$ and Central Au + Au Collisions”, *Phys.Rev.Lett.* **112** no. 12, (2014) 122301, arXiv:1302.6184 [nucl-ex].
- [25] **CMS** Collaboration, V. Khachatryan *et al.*, “Correlations between jets and charged particles in PbPb and pp collisions at $\sqrt{s_{NN}} = 2.76$ TeV”, *JHEP* **02** (2016) 156, arXiv:1601.00079 [nucl-ex].
- [26] **ALICE** Collaboration, S. Acharya *et al.*, “Measurement of jet radial profiles in PbPb collisions at $\sqrt{s_{NN}} = 2.76$ TeV”, *Phys. Lett.* **B796** (2019) 204–219, arXiv:1904.13118 [nucl-ex].
- [27] N. Sharma, J. Mazer, M. Stuart, and C. Natrass, “Background subtraction methods for precision measurements of di-hadron and jet-hadron correlations in heavy ion collisions”, *Phys. Rev.* **C93** no. 4, (2016) 044915, arXiv:1509.04732 [nucl-ex].
- [28] **PHENIX** Collaboration, S. Afanasiev *et al.*, “High- p_T π^0 Production with Respect to the Reaction Plane in Au + Au Collisions at $\sqrt{s_{NN}} = 200$ -GeV”, *Phys.Rev.* **C80** (2009) 054907, arXiv:0903.4886 [nucl-ex].

- [29] **PHENIX** Collaboration, A. Adare *et al.*, “Azimuthal anisotropy of π^0 and η mesons in Au + Au collisions at $\sqrt{s_{NN}} = 200$ GeV”, *Phys. Rev.* **C88** no. 6, (2013) 064910, arXiv:1309.4437 [nucl-ex].
- [30] **ALICE** Collaboration, B. Abelev *et al.*, “Anisotropic flow of charged hadrons, pions and (anti-)protons measured at high transverse momentum in Pb-Pb collisions at $\sqrt{s_{NN}}=2.76$ TeV”, *Phys. Lett.* **B719** (2013) 18–28, arXiv:1205.5761 [nucl-ex].
- [31] **CMS** Collaboration, S. Chatrchyan *et al.*, “Azimuthal anisotropy of charged particles at high transverse momenta in PbPb collisions at $\sqrt{s_{NN}} = 2.76$ TeV”, *Phys. Rev. Lett.* **109** (2012) 022301, arXiv:1204.1850 [nucl-ex].
- [32] **ALICE** Collaboration, S. Acharya *et al.*, “Anisotropic flow of identified particles in Pb-Pb collisions at $\sqrt{s_{NN}} = 5.02$ TeV”, *JHEP* **09** (2018) 006, arXiv:1805.04390 [nucl-ex].
- [33] **ALICE** Collaboration, J. Adam *et al.*, “Azimuthal anisotropy of charged jet production in $\sqrt{s_{NN}} = 2.76$ TeV Pb-Pb collisions”, *Phys. Lett.* **B753** (2016) 511–525, arXiv:1509.07334 [nucl-ex].
- [34] **ATLAS** Collaboration, G. Aad *et al.*, “Measurement of the Azimuthal Angle Dependence of Inclusive Jet Yields in Pb+Pb Collisions at $\sqrt{s_{NN}} = 2.76$ TeV with the ATLAS detector”, *Phys.Rev.Lett.* **111** no. 15, (2013) 152301, arXiv:1306.6469 [hep-ex].
- [35] **PHENIX** Collaboration, A. Adare *et al.*, “Suppression of away-side jet fragments with respect to the reaction plane in Au+Au collisions at $\sqrt{s_{NN}} = 200$ GeV”, *Phys. Rev.* **C84** (2011) 024904, arXiv:1010.1521 [nucl-ex].
- [36] **STAR** Collaboration, H. Agakishiev *et al.*, “Event-plane-dependent dihadron correlations with harmonic v_n subtraction in Au + Au collisions at $\sqrt{s_{NN}} = 200$ GeV”, *Phys. Rev.* **C89** no. 4, (2014) 041901, arXiv:1404.1070 [nucl-ex].
- [37] C. Nattrass, N. Sharma, J. Mazer, M. Stuart, and A. Bejnood, “Disappearance of the Mach Cone in heavy ion collisions”, *Phys. Rev.* **C94** no. 1, (2016) 011901, arXiv:1606.00677 [nucl-ex].
- [38] K. C. Zapp, “Geometrical aspects of jet quenching in JEWEL”, *Phys.Lett.* **B735** (2014) 157–163, arXiv:1312.5536 [hep-ph].
- [39] J. Noronha-Hostler, B. Betz, J. Noronha, and M. Gyulassy, “Event-by-event hydrodynamics + jet energy loss: A solution to the $R_{AA} \otimes v_2$ puzzle”, *Phys. Rev. Lett.* **116** no. 25, (2016) 252301, arXiv:1602.03788 [nucl-th].
- [40] B. Betz, M. Gyulassy, M. Luzum, J. Noronha, J. Noronha-Hostler, I. Portillo, and C. Ratti, “Cumulants and nonlinear response of high p_T harmonic flow at $\sqrt{s_{NN}} = 5.02$ TeV”, *Phys. Rev.* **C95** no. 4, (2017) 044901, arXiv:1609.05171 [nucl-th].
- [41] **ALICE** Collaboration, B. Abelev *et al.*, “Performance of the ALICE Experiment at the CERN LHC”, *Int. J. Mod. Phys.* **A29** (2014) 1430044, arXiv:1402.4476 [nucl-ex].
- [42] **ALICE** Collaboration, E. Abbas *et al.*, “Performance of the ALICE VZERO system”, *JINST* **8** (2013) P10016, arXiv:1306.3130 [nucl-ex].
- [43] **ALICE** Collaboration, P. Cortese *et al.*, “ALICE technical design report on forward detectors: FMD, T0 and V0”,.
- [44] **ALICE** Collaboration, K. Aamodt *et al.*, “Alignment of the ALICE Inner Tracking System with cosmic-ray tracks”, *JINST* **5** (2010) P03003, arXiv:1001.0502 [physics.ins-det].

- [45] J. Alme *et al.*, “The ALICE TPC, a large 3-dimensional tracking device with fast readout for ultra-high multiplicity events”, *Nucl. Instrum. Meth.* **A622** (2010) 316–367, arXiv:1001.1950 [physics.ins-det].
- [46] **ALICE EMCAL** Collaboration, U. Abeyssekara *et al.*, “ALICE EMCAL Physics Performance Report”, arXiv:1008.0413 [physics.ins-det].
- [47] **ALICE** Collaboration, J. Adam *et al.*, “Measurement of jet suppression in central Pb-Pb collisions at $\sqrt{s_{NN}} = 2.76$ TeV”, *Phys. Lett.* **B746** (2015) 1–14, arXiv:1502.01689 [nucl-ex].
- [48] **ALICE** Collaboration, G. Dellacasa *et al.*, “ALICE technical design report of the inner tracking system (ITS)”,.
- [49] **ALICE** Collaboration, G. Dellacasa *et al.*, “ALICE: Technical design report of the time projection chamber”,.
- [50] X.-N. Wang and M. Gyulassy, “HIJING: A Monte Carlo model for multiple jet production in p p, p A and A A collisions”, *Phys. Rev.* **D44** (1991) 3501–3516.
- [51] R. Brun, F. Bruyant, F. Carminati, S. Giani, M. Maire, A. McPherson, G. Patrick, and L. Urban, “GEANT Detector Description and Simulation Tool”,.
- [52] **ALICE** Collaboration, J. Adam *et al.*, “Jet-like correlations with neutral pion triggers in pp and central Pb-Pb collisions at 2.76 TeV”, *Phys. Lett.* **B763** (2016) 238–250, arXiv:1608.07201 [nucl-ex].
- [53] **ALICE** Collaboration, B. Abelev *et al.*, “Measurement of the inclusive differential jet cross section in pp collisions at $\sqrt{s} = 2.76$ TeV”, *Phys. Lett.* **B722** (2013) 262–272, arXiv:1301.3475 [nucl-ex].
- [54] **ALICE** Collaboration, B. *et al.*, “Measurement of charged jet suppression in Pb-Pb collisions at $\sqrt{s_{NN}} = 2.76$ TeV”, *JHEP* **1403** (2014) 013, arXiv:1311.0633 [nucl-ex].
- [55] **ALICE EMCAL** Collaboration, J. Allen *et al.*, “Performance of prototypes for the ALICE electromagnetic calorimeter”, *Nucl. Instrum. Meth.* **A615** (2010) 6–13, arXiv:0912.2005 [physics.ins-det].
- [56] **ALICE** Collaboration, P. Cortese *et al.*, “ALICE electromagnetic calorimeter technical design report”,.
- [57] M. Cacciari, G. P. Salam, and G. Soyez, “FastJet User Manual”, *Eur. Phys. J.* **C72** (2012) 1896, arXiv:1111.6097 [hep-ph].
- [58] **ALICE** Collaboration, B. Abelev *et al.*, “Measurement of Event Background Fluctuations for Charged Particle Jet Reconstruction in Pb-Pb collisions at $\sqrt{s_{NN}} = 2.76$ TeV”, *JHEP* **03** (2012) 053, arXiv:1201.2423 [hep-ex].
- [59] T. Sjostrand, S. Mrenna, and P. Z. Skands, “PYTHIA 6.4 Physics and Manual”, *JHEP* **0605** (2006) 026, arXiv:hep-ph/0603175 [hep-ph].
- [60] **CDF** Collaboration, R. Field and R. C. Group, “PYTHIA tune A, HERWIG, and JIMMY in Run 2 at CDF”, arXiv:hep-ph/0510198 [hep-ph].
- [61] **ALICE** Collaboration, B. *et al.*, “Centrality determination of Pb-Pb collisions at $\sqrt{s_{NN}} = 2.76$ TeV with ALICE”, *Phys. Rev.* **C88** no. 4, (2013) 044909, arXiv:1301.4361 [nucl-ex].

- [62] P. Sorensen, “Implications of space-momentum correlations and geometric fluctuations in heavy-ion collisions”, *J. Phys.* **G37** (2010) 094011, arXiv:1002.4878 [nucl-ex].
- [63] B. Alver and G. Roland, “Collision geometry fluctuations and triangular flow in heavy-ion collisions”, *Phys. Rev.* **C81** (2010) 054905, arXiv:1003.0194 [nucl-th]. [Erratum: *Phys. Rev.* **C82**, 039903(2010)].
- [64] A. M. Poskanzer and S. Voloshin, “Methods for analyzing anisotropic flow in relativistic nuclear collisions”, *Phys. Rev.* **C58** (1998) 1671–1678, arXiv:nucl-ex/9805001 [nucl-ex].
- [65] **E877** Collaboration, J. Barrette *et al.*, “Energy and charged particle flow in a 10.8-A/GeV/c Au + Au collisions”, *Phys. Rev.* **C55** (1997) 1420–1430, arXiv:nucl-ex/9610006 [nucl-ex].
- [66] J. Bielcikova, S. Esumi, K. Filimonov, S. Voloshin, and J. Wurm, “Elliptic flow contribution to two particle correlations at different orientations to the reaction plane”, *Phys. Rev.* **C69** (2004) 021901, arXiv:nucl-ex/0311007 [nucl-ex].
- [67] C. Nattrass and T. Todoroki, “Event plane dependence of the flow modulated background in dihadron and jet-hadron correlations in heavy ion collisions”, *Phys. Rev.* **C97** no. 5, (2018) 054911, arXiv:1802.01668 [nucl-ex].
- [68] **ATLAS** Collaboration, G. Aad *et al.*, “Measurement of event-plane correlations in $\sqrt{s_{NN}} = 2.76$ TeV lead-lead collisions with the ATLAS detector”, *Phys. Rev.* **C90** no. 2, (2014) 024905, arXiv:1403.0489 [hep-ex].
- [69] M. Luzum and J.-Y. Ollitrault, “Directed flow at midrapidity in heavy-ion collisions”, *Phys. Rev. Lett.* **106** (2011) 102301, arXiv:1011.6361 [nucl-ex].
- [70] **ATLAS** Collaboration, G. Aad *et al.*, “Measurement of the azimuthal anisotropy for charged particle production in $\sqrt{s_{NN}} = 2.76$ TeV lead-lead collisions with the ATLAS detector”, *Phys. Rev.* **C86** (2012) 014907, arXiv:1203.3087 [hep-ex].
- [71] **ALICE** Collaboration, “Second order event plane dependence of jet-hadron correlations in Pb-Pb collisions at $\sqrt{s_{NN}} = 2.76$ TeV”, <https://cds.cern.ch/record/2696428>. ALICE-PUBLIC-2019-004.
- [72] **PHENIX** Collaboration, A. Adare *et al.*, “Measurement of two-particle correlations with respect to second- and third-order event planes in Au+Au collisions at $\sqrt{s_{NN}} = 200$ GeV”, *Phys. Rev.* **C99** no. 5, (2019) 054903, arXiv:1803.01749 [hep-ex].
- [73] K. C. Zapp, “JEWEL 2.0.0: directions for use”, *Eur. Phys. J.* **C74** no. 2, (2014) 2762, arXiv:1311.0048 [hep-ph].
- [74] J. G. Milhano and K. C. Zapp, “Origins of the di-jet asymmetry in heavy ion collisions”, *Eur. Phys. J.* **C76** no. 5, (2016) 288, arXiv:1512.08107 [hep-ph].

A The ALICE Collaboration

S. Acharya¹⁴¹, D. Adamová⁹³, A. Adler⁷³, J. Adolfsson⁷⁹, M.M. Aggarwal⁹⁸, G. Aglieri Rinella³⁴, M. Agnello³¹, N. Agrawal^{10,53}, Z. Ahammed¹⁴¹, S. Ahmad¹⁷, S.U. Ahn⁷⁵, A. Akindinov⁹⁰, M. Al-Turany¹⁰⁵, S.N. Alam¹⁴¹, D.S.D. Albuquerque¹²², D. Aleksandrov⁸⁶, B. Alessandro⁵⁸, H.M. Alfanda⁶, R. Alfaro Molina⁷¹, B. Ali¹⁷, Y. Ali¹⁵, A. Alici^{10,27,53}, A. Alkin², J. Alme²², T. Alt⁶⁸, L. Altenkamper²², I. Altsybeev¹¹², M.N. Anaam⁶, C. Andrei⁴⁷, D. Andreou³⁴, H.A. Andrews¹⁰⁹, A. Andronic¹⁴⁴, M. Angeletti³⁴, V. Anguelov¹⁰², C. Anson¹⁶, T. Antičić¹⁰⁶, F. Antinori⁵⁶, P. Antonioli⁵³, R. Anwar¹²⁵, N. Apadula⁷⁸, L. Aphecetche¹¹⁴, H. Appelshäuser⁶⁸, S. Arcelli²⁷, R. Arnaldi⁵⁸, M. Arratia⁷⁸, I.C. Arsene²¹, M. Arslanok¹⁰², A. Augustinus³⁴, R. Averbeck¹⁰⁵, S. Aziz⁶¹, M.D. Azmi¹⁷, A. Badalà⁵⁵, Y.W. Baek⁴⁰, S. Bagnasco⁵⁸, X. Bai¹⁰⁵, R. Bailhache⁶⁸, R. Bala⁹⁹, A. Baldisseri¹³⁷, M. Ball⁴², S. Balouza¹⁰³, R. Barbera²⁸, L. Barioglio²⁶, G.G. Barnaföldi¹⁴⁵, L.S. Barnby⁹², V. Barret¹³⁴, P. Bartalini⁶, K. Barth³⁴, E. Bartsch⁶⁸, F. Baruffaldi²⁹, N. Bastid¹³⁴, S. Basu¹⁴³, G. Batigne¹¹⁴, B. Batyunya⁷⁴, D. Bauri⁴⁸, J.L. Bazo Alba¹¹⁰, I.G. Bearden⁸⁷, C. Bedda⁶³, N.K. Behera⁶⁰, I. Belikov¹³⁶, A.D.C. Bell Hechavarria¹⁴⁴, F. Bellini³⁴, R. Bellwied¹²⁵, V. Belyaev⁹¹, G. Bencedi¹⁴⁵, S. Beole²⁶, A. Bercuci⁴⁷, Y. Berdnikov⁹⁶, D. Berenyi¹⁴⁵, R.A. Bertens¹³⁰, D. Berzano⁵⁸, M.G. Besoiu⁶⁷, L. Betev³⁴, A. Bhasin⁹⁹, I.R. Bhat⁹⁹, M.A. Bhat³, H. Bhatt⁴⁸, B. Bhattacharjee⁴¹, A. Bianchi²⁶, L. Bianchi²⁶, N. Bianchi⁵¹, J. Bielčič³⁷, J. Bielčíková⁹³, A. Bilandžić^{103,117}, G. Biro¹⁴⁵, R. Biswas³, S. Biswas³, J.T. Blair¹¹⁹, D. Blau⁸⁶, C. Blume⁶⁸, G. Boca¹³⁹, F. Bock^{34,94}, A. Bogdanov⁹¹, L. Boldizsár¹⁴⁵, A. Bolozdynya⁹¹, M. Bombara³⁸, G. Bonomi¹⁴⁰, H. Borel¹³⁷, A. Borissov^{91,144}, H. Bossi¹⁴⁶, E. Botta²⁶, L. Bratrud⁶⁸, P. Braun-Munzinger¹⁰⁵, M. Bregant¹²¹, T.A. Broker⁶⁸, M. Broz³⁷, E.J. Brucken⁴³, E. Bruna⁵⁸, G.E. Bruno¹⁰⁴, M.D. Buckland¹²⁷, D. Budnikov¹⁰⁷, H. Buesching⁶⁸, S. Bufalino³¹, O. Bugnon¹¹⁴, P. Buhler¹¹³, P. Buncic³⁴, Z. Buthelezi^{72,131}, J.B. Butt¹⁵, J.T. Buxton⁹⁵, S.A. Bysiak¹¹⁸, D. Caffarri⁸⁸, A. Caliva¹⁰⁵, E. Calvo Villar¹¹⁰, R.S. Camacho⁴⁴, P. Camerini²⁵, A.A. Capon¹¹³, F. Carnesecchi^{10,27}, R. Caron¹³⁷, J. Castillo Castellanos¹³⁷, A.J. Castro¹³⁰, E.A.R. Casula⁵⁴, F. Catalano³¹, C. Ceballos Sanchez⁵², P. Chakraborty⁴⁸, S. Chandra¹⁴¹, W. Chang⁶, S. Chapeland³⁴, M. Chartier¹²⁷, S. Chattopadhyay¹⁴¹, S. Chattopadhyay¹⁰⁸, A. Chauvin²⁴, C. Cheshkov¹³⁵, B. Cheynis¹³⁵, V. Chibante Barroso³⁴, D.D. Chinellato¹²², S. Cho⁶⁰, P. Chochula³⁴, T. Chowdhury¹³⁴, P. Christakoglou⁸⁸, C.H. Christensen⁸⁷, P. Christiansen⁷⁹, T. Chujo¹³³, C. Cicalo⁵⁴, L. Cifarelli^{10,27}, F. Cindolo⁵³, J. Cleymans¹²⁴, F. Colamaria⁵², D. Colella⁵², A. Collu⁷⁸, M. Colocci²⁷, M. Concas^{58,ii}, G. Conesa Balbastre⁷⁷, Z. Conesa del Valle⁶¹, G. Contin^{59,127}, J.G. Contreras³⁷, T.M. Cormier⁹⁴, Y. Corrales Morales^{26,58}, P. Cortese³², M.R. Cosentino¹²³, F. Costa³⁴, S. Costanza¹³⁹, P. Crochet¹³⁴, E. Cuautele⁶⁹, P. Cui⁶, L. Cunqueiro⁹⁴, D. Dabrowski¹⁴², T. Dahms^{103,117}, A. Dainese⁵⁶, F.P.A. Damas^{114,137}, M.C. Danisch¹⁰², A. Danu⁶⁷, D. Das¹⁰⁸, I. Das¹⁰⁸, P. Das⁸⁴, P. Das³, S. Das³, A. Dash⁸⁴, S. Dash⁴⁸, A. Dashi¹⁰³, S. De⁸⁴, A. De Caro³⁰, G. de Cataldo⁵², C. de Conti¹²¹, J. de Cuveland³⁹, A. De Falco²⁴, D. De Gruttola¹⁰, N. De Marco⁵⁸, S. De Pasquale³⁰, S. Deb⁴⁹, B. Debjani³, H.F. Degenhardt¹²¹, K.R. Deja¹⁴², A. Deloff⁸³, S. Delsanto^{26,131}, D. Devetak¹⁰⁵, P. Dhankher⁴⁸, D. Di Bari³³, A. Di Mauro³⁴, R.A. Diaz⁸, T. Dietel¹²⁴, P. Dillenseger⁶⁸, Y. Ding⁶, R. Divià³⁴, Ø. Djuvsland²², U. Dmitrieva⁶², A. Dobrin^{34,67}, B. Dönigus⁶⁸, O. Dordic²¹, A.K. Dubey¹⁴¹, A. Dubla¹⁰⁵, S. Dudi⁹⁸, M. Dukhishyam⁸⁴, P. Dupieux¹³⁴, R.J. Ehlers¹⁴⁶, V.N. Eikeland²², D. Elia⁵², H. Engel⁷³, E. Eppe¹⁴⁶, B. Erazmus¹¹⁴, F. Erhardt⁹⁷, A. Erokhin¹¹², M.R. Ersdal²², B. Espagnon⁶¹, G. Eulisse³⁴, D. Evans¹⁰⁹, S. Evdokimov⁸⁹, L. Fabbietti^{103,117}, M. Faggin²⁹, J. Faivre⁷⁷, F. Fan⁶, A. Fantoni⁵¹, M. Fasel⁹⁴, P. Fedichio³¹, A. Feliciello⁵⁸, G. Feofilov¹¹², A. Fernández Téllez⁴⁴, A. Ferrero¹³⁷, A. Ferretti²⁶, A. Festanti³⁴, V.J.G. Feuillard¹⁰², J. Figiel¹¹⁸, S. Filchagin¹⁰⁷, D. Finogeev⁶², F.M. Fionda²², G. Fiorenza⁵², F. Flor¹²⁵, S. Foertsch⁷², P. Foka¹⁰⁵, S. Fokin⁸⁶, E. Fragiaco⁵⁹, U. Frankenfeld¹⁰⁵, U. Fuchs³⁴, C. Furget⁷⁷, A. Furs⁶², M. Fusco Girard³⁰, J.J. Gaardhøje⁸⁷, M. Gagliardi²⁶, A.M. Gago¹¹⁰, A. Gal¹³⁶, C.D. Galvan¹²⁰, P. Ganoti⁸², C. Garabatos¹⁰⁵, E. Garcia-Solis¹¹, K. Garg²⁸, C. Gargiulo³⁴, A. Garibli⁸⁵, K. Garner¹⁴⁴, P. Gasik^{103,117}, E.F. Gauger¹¹⁹, M.B. Gay Ducati⁷⁰, M. Germain¹¹⁴, J. Ghosh¹⁰⁸, P. Ghosh¹⁴¹, S.K. Ghosh³, P. Gianotti⁵¹, P. Giubellino^{58,105}, P. Giubilato²⁹, P. Glässel¹⁰², D.M. Gómez Coral⁷¹, A. Gomez Ramirez⁷³, V. Gonzalez¹⁰⁵, P. González-Zamora⁴⁴, S. Gorbunov³⁹, L. Görlich¹¹⁸, S. Gotovac³⁵, V. Grabski⁷¹, L.K. Graczykowski¹⁴², K.L. Graham¹⁰⁹, L. Greiner⁷⁸, A. Grelli⁶³, C. Grigoras³⁴, V. Grigoriev⁹¹, A. Grigoryan¹, S. Grigoryan⁷⁴, O.S. Groettvik²², F. Grosa³¹, J.F. Grosse-Oetringhaus³⁴, R. Grosso¹⁰⁵, R. Guernane⁷⁷, M. Guittiere¹¹⁴, K. Gulbrandsen⁸⁷, T. Gunji¹³², A. Gupta⁹⁹, R. Gupta⁹⁹, I.B. Guzman⁴⁴, R. Haake¹⁴⁶, M.K. Habib¹⁰⁵, C. Hadjidakis⁶¹, H. Hamagaki⁸⁰, G. Hamar¹⁴⁵, M. Hamid⁶, R. Hannigan¹¹⁹, M.R. Haque^{63,84}, A. Harlanderova¹⁰⁵, J.W. Harris¹⁴⁶, A. Harton¹¹, J.A. Hasenbichler³⁴, D. Hatzifotiadou^{10,53}, P. Hauer⁴², S. Hayashi¹³², S.T. Heckel^{68,103}, E. Hellbär⁶⁸, H. Helstrup³⁶, A. Hergelegiu⁴⁷, E.G. Hernandez⁴⁴, G. Herrera Corral⁹, F. Herrmann¹⁴⁴, K.F. Hetland³⁶, T.E. Hilden⁴³, H. Hillemanns³⁴, C. Hills¹²⁷, B. Hippolyte¹³⁶, B. Hohlweger¹⁰³, D. Horak³⁷, A. Hornung⁶⁸, S. Hornung¹⁰⁵, R. Hosokawa^{16,133}, P. Hristov³⁴, C. Huang⁶¹, C. Hughes¹³⁰, P. Huhn⁶⁸, T.J. Humanic⁹⁵, H. Hushnud¹⁰⁸,

L.A. Husova¹⁴⁴, N. Hussain⁴¹, S.A. Hussain¹⁵, D. Hutter³⁹, J.P. Iddon^{34,127}, R. Ilkaev¹⁰⁷, M. Inaba¹³³,
 G.M. Innocenti³⁴, M. Ippolitov⁸⁶, A. Isakov⁹³, M.S. Islam¹⁰⁸, M. Ivanov¹⁰⁵, V. Ivanov⁹⁶, V. Izucheev⁸⁹,
 B. Jacak⁷⁸, N. Jacazio^{27,53}, P.M. Jacobs⁷⁸, M.B. Jadhav⁴⁸, S. Jadlovská¹¹⁶, J. Jadlovsky¹¹⁶, S. Jaelani⁶³,
 C. Jahnke¹²¹, M.J. Jakubowska¹⁴², M.A. Janik¹⁴², T. Janson⁷³, M. Jercic⁹⁷, O. Jevons¹⁰⁹, M. Jin¹²⁵,
 F. Jonas^{94,144}, P.G. Jones¹⁰⁹, J. Jung⁶⁸, M. Jung⁶⁸, A. Jusko¹⁰⁹, P. Kalinak⁶⁴, A. Kalweit³⁴, V. Kaplin⁹¹,
 S. Kar⁶, A. Karasu Uysal⁷⁶, O. Karavichev⁶², T. Karavicheva⁶², P. Karczmarczyk³⁴, E. Karpechev⁶²,
 U. Kebschull⁷³, R. Keidel⁴⁶, M. Keil³⁴, B. Ketzer⁴², Z. Khabanova⁸⁸, A.M. Khan⁶, S. Khan¹⁷, S.A. Khan¹⁴¹,
 A. Khanzadeev⁹⁶, Y. Kharlov⁸⁹, A. Khatun¹⁷, A. Khuntia¹¹⁸, B. Kileng³⁶, B. Kim⁶⁰, B. Kim¹³³, D. Kim¹⁴⁷,
 D.J. Kim¹²⁶, E.J. Kim¹³, H. Kim^{18,147}, J. Kim¹⁴⁷, J.S. Kim⁴⁰, J. Kim¹⁰², J. Kim¹⁴⁷, J. Kim¹³, M. Kim¹⁰²,
 S. Kim¹⁹, T. Kim¹⁴⁷, T. Kim¹⁴⁷, S. Kirsch^{39,68}, I. Kisel³⁹, S. Kiselev⁹⁰, A. Kisiel¹⁴², J.L. Klay⁵, C. Klein⁶⁸,
 J. Klein⁵⁸, S. Klein⁷⁸, C. Klein-Bösing¹⁴⁴, M. Kleiner⁶⁸, S. Klewin¹⁰², A. Kluge³⁴, M.L. Knichel³⁴,
 A.G. Knospe¹²⁵, C. Kobdaj¹¹⁵, M.K. Köhler¹⁰², T. Kollegger¹⁰⁵, A. Kondratyev⁷⁴, N. Kondratyeva⁹¹,
 E. Kondratyuk⁸⁹, J. König⁶⁸, P.J. Konopka³⁴, L. Koska¹¹⁶, O. Kovalenko⁸³, V. Kovalenko¹¹², M. Kowalski¹¹⁸,
 I. Králik⁶⁴, A. Kravčáková³⁸, L. Kreis¹⁰⁵, M. Krivda^{64,109}, F. Krizek⁹³, K. Krizkova Gajdosova³⁷,
 M. Krüger⁶⁸, E. Kryshen⁹⁶, M. Krzewicki³⁹, A.M. Kubera⁹⁵, V. Kučera⁶⁰, C. Kuhn¹³⁶, P.G. Kuijer⁸⁸,
 L. Kumar⁹⁸, S. Kumar⁴⁸, S. Kundu⁸⁴, P. Kurashvili⁸³, A. Kurepin⁶², A.B. Kurepin⁶², A. Kuryakin¹⁰⁷,
 S. Kushpil⁹³, J. Kvapil¹⁰⁹, M.J. Kweon⁶⁰, J.Y. Kwon⁶⁰, Y. Kwon¹⁴⁷, S.L. La Pointe³⁹, P. La Rocca²⁸,
 Y.S. Lai⁷⁸, R. Langoy¹²⁹, K. Lapidus³⁴, A. Lardeux²¹, P. Larionov⁵¹, E. Laudi³⁴, R. Lavicka³⁷,
 T. Lazareva¹¹², R. Lea²⁵, L. Leardini¹⁰², J. Lee¹³³, S. Lee¹⁴⁷, F. Lehas⁸⁸, S. Lehner¹¹³, J. Lehrbach³⁹,
 R.C. Lemmon⁹², I. León Monzón¹²⁰, E.D. Lesser²⁰, M. Lettrich³⁴, P. Lévai¹⁴⁵, X. Li¹², X.L. Li⁶, J. Lien¹²⁹,
 R. Lietava¹⁰⁹, B. Lim¹⁸, V. Lindenstruth³⁹, S.W. Lindsay¹²⁷, C. Lippmann¹⁰⁵, M.A. Lisa⁹⁵, V. Litichevskiy⁴³,
 A. Liu⁷⁸, S. Liu⁹⁵, W.J. Llope¹⁴³, I.M. Lofnes²², V. Loginov⁹¹, C. Loizides⁹⁴, P. Loncar³⁵, X. Lopez¹³⁴,
 E. López Torres⁸, J.R. Luhder¹⁴⁴, M. Lunardon²⁹, G. Luparello⁵⁹, Y. Ma¹¹¹, A. Maevskaya⁶², M. Mager³⁴,
 S.M. Mahmood²¹, T. Mahmoud⁴², A. Maire¹³⁶, R.D. Majka¹⁴⁶, M. Malaev⁹⁶, Q.W. Malik²¹, L. Malinina^{74,iii},
 D. Mal'Kevich⁹⁰, P. Malzacher¹⁰⁵, G. Mandaglio⁵⁵, V. Manko⁸⁶, F. Manso¹³⁴, V. Manzari⁵², Y. Mao⁶,
 M. Marchisone¹³⁵, J. Mareš⁶⁶, G.V. Margagliotti²⁵, A. Margotti⁵³, J. Margutti⁶³, A. Marín¹⁰⁵, C. Markert¹¹⁹,
 M. Marquard⁶⁸, N.A. Martin¹⁰², P. Martinengo³⁴, J.L. Martinez¹²⁵, M.I. Martínez⁴⁴, G. Martínez García¹¹⁴,
 M. Martinez Pedreira³⁴, S. Masciocchi¹⁰⁵, M. Masera²⁶, A. Masoni⁵⁴, L. Massacrier⁶¹, E. Masson¹¹⁴,
 A. Mastroserio^{52,138}, A.M. Mathis^{103,117}, O. Matonoha⁷⁹, P.F.T. Matuoka¹²¹, A. Matyja¹¹⁸, C. Mayer¹¹⁸,
 M. Mazzilli³³, M.A. Mazzoni⁵⁷, A.F. Mechler⁶⁸, F. Meddi²³, Y. Melikyan^{62,91}, A. Menchaca-Rocha⁷¹,
 C. Mengke⁶, E. Meninno^{30,113}, M. Meres¹⁴, S. Mhlanga¹²⁴, Y. Miake¹³³, L. Micheletti²⁶, D.L. Mihaylov¹⁰³,
 K. Mikhaylov^{74,90}, A. Mischke^{63,i}, A.N. Mishra⁶⁹, D. Miśkowiec¹⁰⁵, A. Modak³, N. Mohammadi³⁴,
 A.P. Mohanty⁶³, B. Mohanty⁸⁴, M. Mohisin Khan^{17,iv}, C. Mordasini¹⁰³, D.A. Moreira De Godoy¹⁴⁴,
 L.A.P. Moreno⁴⁴, I. Morozov⁶², A. Morsch³⁴, T. Mrnjavac³⁴, V. Muccifora⁵¹, E. Mudnic³⁵, D. Mühlheim¹⁴⁴,
 S. Muhuri¹⁴¹, J.D. Mulligan⁷⁸, M.G. Munhoz¹²¹, K. Münnig⁴², R.H. Munzer⁶⁸, H. Murakami¹³²,
 S. Murray¹²⁴, L. Musa³⁴, J. Musinsky⁶⁴, C.J. Myers¹²⁵, J.W. Myrcha¹⁴², B. Naik⁴⁸, R. Nair⁸³, B.K. Nandi⁴⁸,
 R. Nania^{10,53}, E. Nappi⁵², M.U. Naru¹⁵, A.F. Nassirpour⁷⁹, C. Nattrass¹³⁰, R. Nayak⁴⁸, T.K. Nayak⁸⁴,
 S. Nazarenko¹⁰⁷, A. Neagu²¹, R.A. Negrao De Oliveira⁶⁸, L. Nellen⁶⁹, S.V. Nesbo³⁶, G. Neskovic³⁹,
 D. Nesterov¹¹², L.T. Neumann¹⁴², B.S. Nielsen⁸⁷, S. Nikolaev⁸⁶, S. Nikulin⁸⁶, V. Nikulin⁹⁶, F. Noferini^{10,53},
 P. Nomokonov⁷⁴, J. Norman⁷⁷, N. Novitzky¹³³, P. Nowakowski¹⁴², A. Nyanin⁸⁶, J. Nystrand²², M. Ogino⁸⁰,
 A. Ohlson^{79,102}, J. Olińczak¹⁴², A.C. Oliveira Da Silva^{121,130}, M.H. Oliver¹⁴⁶, C. Oppedisano⁵⁸, R. Orava⁴³,
 A. Ortiz Velasquez⁶⁹, A. Oskarsson⁷⁹, J. Otwinowski¹¹⁸, K. Oyama⁸⁰, Y. Pachmayer¹⁰², V. Pacik⁸⁷,
 D. Pagano¹⁴⁰, G. Paic⁶⁹, J. Pan¹⁴³, A.K. Pandey⁴⁸, S. Panebianco¹³⁷, P. Pareek^{49,141}, J. Park⁶⁰,
 J.E. Parkkila¹²⁶, S. Parmar⁹⁸, S.P. Pathak¹²⁵, R.N. Patra¹⁴¹, B. Paul^{24,58}, H. Pei⁶, T. Peitzmann⁶³, X. Peng⁶,
 L.G. Pereira⁷⁰, H. Pereira Da Costa¹³⁷, D. Peresunko⁸⁶, G.M. Perez⁸, E. Perez Lezama⁶⁸, V. Peskov⁶⁸,
 Y. Pestov⁴, V. Petráček³⁷, M. Petrovici⁴⁷, R.P. Pezzi⁷⁰, S. Piano⁵⁹, M. Pikna¹⁴, P. Pillot¹¹⁴,
 L.O.D.L. Pimentel⁸⁷, O. Pinazza^{34,53}, L. Pinsky¹²⁵, C. Pinto²⁸, S. Pisano^{10,51}, D. Pistone⁵⁵, M. Płoskoń⁷⁸,
 M. Planinic⁹⁷, F. Pliquett⁶⁸, J. Pluta¹⁴², S. Pochybova^{145,i}, M.G. Poghosyan⁹⁴, B. Polichtchouk⁸⁹, N. Poljak⁹⁷,
 A. Pop⁴⁷, H. Poppenborg¹⁴⁴, S. Porteboeuf-Houssais¹³⁴, V. Pozdniakov⁷⁴, S.K. Prasad³, R. Preghenella⁵³,
 F. Prino⁵⁸, C.A. Pruneau¹⁴³, I. Pshenichnov⁶², M. Puccio^{26,34}, V. Punin¹⁰⁷, J. Putschke¹⁴³, R.E. Quishpe¹²⁵,
 S. Ragoni¹⁰⁹, S. Raha³, S. Rajput⁹⁹, J. Rak¹²⁶, A. Rakotozafindrabe¹³⁷, L. Ramello³², F. Rami¹³⁶,
 R. Raniwala¹⁰⁰, S. Raniwala¹⁰⁰, S.S. Räsänen⁴³, R. Rath⁴⁹, V. Ratzka⁴², I. Ravasenga³¹, K.F. Read^{94,130},
 K. Redlich^{83,v}, A. Rehman²², P. Reichelt⁶⁸, F. Reidt³⁴, X. Ren⁶, R. Renfordt⁶⁸, Z. Rescakova³⁸, J.-P. Revol¹⁰,
 K. Reygers¹⁰², V. Riabov⁹⁶, T. Richert^{79,87}, M. Richter²¹, P. Riedler³⁴, W. Riegler³⁴, F. Riggi²⁸, C. Ristea⁶⁷,
 S.P. Rode⁴⁹, M. Rodríguez Cahuantzi⁴⁴, K. Røed²¹, R. Rogalev⁸⁹, E. Rogochaya⁷⁴, D. Rohr³⁴, D. Röhrich²²,
 P.S. Rokita¹⁴², F. Ronchetti⁵¹, E.D. Rosas⁶⁹, K. Roslon¹⁴², A. Rossi^{29,56}, A. Rotondi¹³⁹, F. Roukoutakis⁸²,

A. Roy⁴⁹, P. Roy¹⁰⁸, O.V. Rueda⁷⁹, R. Rui²⁵, B. Rumyantsev⁷⁴, A. Rustamov⁸⁵, E. Ryabinkin⁸⁶, Y. Ryabov⁹⁶, A. Rybicki¹¹⁸, H. Rytönen¹²⁶, S. Sadhu¹⁴¹, S. Sadovsky⁸⁹, K. Šafařík^{34,37}, S.K. Saha¹⁴¹, B. Sahoo⁴⁸, P. Sahoo^{48,49}, R. Sahoo⁴⁹, S. Sahoo⁶⁵, P.K. Sahu⁶⁵, J. Saini¹⁴¹, S. Sakai¹³³, S. Sambyal⁹⁹, V. Samsonov^{91,96}, D. Sarkar¹⁴³, N. Sarkar¹⁴¹, P. Sarma⁴¹, V.M. Sarti¹⁰³, M.H.P. Sas⁶³, E. Scapparone⁵³, B. Schaefer⁹⁴, J. Schambach¹¹⁹, H.S. Scheid⁶⁸, C. Schiaua⁴⁷, R. Schicker¹⁰², A. Schmah¹⁰², C. Schmidt¹⁰⁵, H.R. Schmidt¹⁰¹, M.O. Schmidt¹⁰², M. Schmidt¹⁰¹, N.V. Schmidt^{68,94}, A.R. Schmier¹³⁰, J. Schukraft⁸⁷, Y. Schutz^{34,136}, K. Schwarz¹⁰⁵, K. Schweda¹⁰⁵, G. Scioli²⁷, E. Scomparin⁵⁸, M. Šefčík³⁸, J.E. Seger¹⁶, M.E. Connors¹⁴⁶, J.A. Mazer¹³⁰, Y. Sekiguchi¹³², D. Sekihata^{45,132}, I. Selyuzhenkov^{91,105}, S. Senyukov¹³⁶, D. Serebryakov⁶², E. Serradilla⁷¹, A. Sevcenco⁶⁷, A. Shabanov⁶², A. Shabetai¹¹⁴, R. Shahoyan³⁴, W. Shaikh¹⁰⁸, A. Shangaraev⁸⁹, A. Sharma⁹⁸, A. Sharma⁹⁹, H. Sharma¹¹⁸, M. Sharma⁹⁹, N. Sharma⁹⁸, A.I. Sheikh¹⁴¹, K. Shigaki⁴⁵, M. Shimomura⁸¹, S. Shirinkin⁹⁰, Q. Shou¹¹¹, Y. Sibiriak⁸⁶, S. Siddhanta⁵⁴, T. Siemiarczuk⁸³, D. Silvermyr⁷⁹, G. Simatovic⁸⁸, G. Simonetti^{34,103}, R. Singh⁸⁴, R. Singh⁹⁹, R. Singh⁴⁹, V.K. Singh¹⁴¹, V. Singhal¹⁴¹, T. Sinha¹⁰⁸, B. Sitar¹⁴, M. Sitta³², T.B. Skaali²¹, M. Slupecki¹²⁶, N. Smirnov¹⁴⁶, R.J.M. Snellings⁶³, T.W. Snellman^{43,126}, C. Soncco¹¹⁰, J. Song^{60,125}, A. Songmoolnak¹¹⁵, F. Soramel²⁹, S. Sorensen¹³⁰, I. Sputowska¹¹⁸, J. Stachel¹⁰², I. Stan⁶⁷, P. Stankus⁹⁴, P.J. Steffanic¹³⁰, E. Stenlund⁷⁹, D. Stocco¹¹⁴, M.M. Storetvedt³⁶, L.D. Stritto³⁰, A.A.P. Suaide¹²¹, T. Sugitate⁴⁵, C. Suire⁶¹, M. Suleymanov¹⁵, M. Suljic³⁴, R. Sultanov⁹⁰, M. Šumbera⁹³, S. Sumowidagdo⁵⁰, S. Swain⁶⁵, A. Szabo¹⁴, I. Szarka¹⁴, U. Tabassam¹⁵, G. Taillepied¹³⁴, J. Takahashi¹²², G.J. Tambave²², S. Tang^{6,134}, M. Tarhini¹¹⁴, M.G. Tarzila⁴⁷, A. Tauro³⁴, G. Tejada Muñoz⁴⁴, A. Telesca³⁴, C. Terrevoli¹²⁵, D. Thakur⁴⁹, S. Thakur¹⁴¹, D. Thomas¹¹⁹, F. Thoresen⁸⁷, R. Tieulent¹³⁵, A. Tikhonov⁶², A.R. Timmins¹²⁵, A. Toia⁶⁸, N. Topilskaya⁶², M. Toppi⁵¹, F. Torres-Acosta²⁰, S.R. Torres^{9,120}, A. Trifiro⁵⁵, S. Tripathy⁴⁹, T. Tripathy⁴⁸, S. Trogolo²⁹, G. Trombetta³³, L. Tropp³⁸, V. Trubnikov², W.H. Trzaska¹²⁶, T.P. Trzcinski¹⁴², B.A. Trzeciak⁶³, T. Tsuji¹³², A. Tumkin¹⁰⁷, R. Turrisi⁵⁶, T.S. Tveter²¹, K. Ullaland²², E.N. Umaka¹²⁵, A. Uras¹³⁵, G.L. Usai²⁴, A. Utrobicic⁹⁷, M. Vala³⁸, N. Valle¹³⁹, S. Vallero⁵⁸, N. van der Kolk⁶³, L.V.R. van Doremalen⁶³, M. van Leeuwen⁶³, P. Vande Vyvre³⁴, D. Varga¹⁴⁵, Z. Varga¹⁴⁵, M. Varga-Kofarago¹⁴⁵, A. Vargas⁴⁴, M. Vargyas¹²⁶, M. Vasileiou⁸², A. Vasiliev⁸⁶, O. Vázquez Doce^{103,117}, V. Vechernin¹¹², A.M. Veen⁶³, E. Vercellin²⁶, S. Vergara Limón⁴⁴, L. Vermunt⁶³, R. Vernet⁷, R. Vértesi¹⁴⁵, L. Vickovic³⁵, J. Viinikainen¹²⁶, Z. Vilakazi¹³¹, O. Villalobos Baillie¹⁰⁹, A. Villatoro Tello⁴⁴, G. Vino⁵², A. Vinogradov⁸⁶, T. Virgili³⁰, V. Vislavicius⁸⁷, A. Vodopyanov⁷⁴, B. Volkel³⁴, M.A. Völkl¹⁰¹, K. Voloshin⁹⁰, S.A. Voloshin¹⁴³, G. Volpe³³, B. von Haller³⁴, I. Vorobyev¹⁰³, D. Voscek¹¹⁶, J. Vrláková³⁸, B. Wagner²², M. Weber¹¹³, S.G. Weber^{105,144}, A. Wegrzynek³⁴, D.F. Weiser¹⁰², S.C. Wenzel³⁴, J.P. Wessels¹⁴⁴, J. Wiechula⁶⁸, J. Wikne²¹, G. Wilk⁸³, J. Wilkinson^{10,53}, G.A. Willems³⁴, E. Willsher¹⁰⁹, B. Windelband¹⁰², W.E. Witt¹³⁰, Y. Wu¹²⁸, R. Xu⁶, S. Yalcin⁷⁶, K. Yamakawa⁴⁵, S. Yang²², S. Yano¹³⁷, Z. Yin⁶, H. Yokoyama⁶³, I.-K. Yoo¹⁸, J.H. Yoon⁶⁰, S. Yuan²², A. Yuncu¹⁰², V. Yurchenko², V. Zaccolo²⁵, A. Zaman¹⁵, C. Zampolli³⁴, H.J.C. Zanoli^{63,121}, N. Zardoshti³⁴, A. Zarochentsev¹¹², P. Závada⁶⁶, N. Zaviyalov¹⁰⁷, H. Zbroszczyk¹⁴², M. Zhalov⁹⁶, S. Zhang¹¹¹, X. Zhang⁶, Z. Zhang⁶, V. Zhrebchevskii¹¹², N. Zhigareva⁹⁰, D. Zhou⁶, Y. Zhou⁸⁷, Z. Zhou²², J. Zhu^{6,105}, Y. Zhu⁶, A. Zichichi^{10,27}, M.B. Zimmermann³⁴, G. Zinovjev², N. Zurlo¹⁴⁰,

Affiliation notes

ⁱ Deceased

ⁱⁱ Dipartimento DET del Politecnico di Torino, Turin, Italy

ⁱⁱⁱ M.V. Lomonosov Moscow State University, D.V. Skobeltsyn Institute of Nuclear Physics, Moscow, Russia

^{iv} Department of Applied Physics, Aligarh Muslim University, Aligarh, India

^v Institute of Theoretical Physics, University of Wrocław, Poland

Collaboration Institutes

¹ A.I. Alikhanyan National Science Laboratory (Yerevan Physics Institute) Foundation, Yerevan, Armenia

² Bogolyubov Institute for Theoretical Physics, National Academy of Sciences of Ukraine, Kiev, Ukraine

³ Bose Institute, Department of Physics and Centre for Astroparticle Physics and Space Science (CAPSS), Kolkata, India

⁴ Budker Institute for Nuclear Physics, Novosibirsk, Russia

⁵ California Polytechnic State University, San Luis Obispo, California, United States

⁶ Central China Normal University, Wuhan, China

⁷ Centre de Calcul de l'IN2P3, Villeurbanne, Lyon, France

⁸ Centro de Aplicaciones Tecnológicas y Desarrollo Nuclear (CEADEN), Havana, Cuba

- ⁹ Centro de Investigación y de Estudios Avanzados (CINVESTAV), Mexico City and Mérida, Mexico
- ¹⁰ Centro Fermi - Museo Storico della Fisica e Centro Studi e Ricerche “Enrico Fermi”, Rome, Italy
- ¹¹ Chicago State University, Chicago, Illinois, United States
- ¹² China Institute of Atomic Energy, Beijing, China
- ¹³ Chonbuk National University, Jeonju, Republic of Korea
- ¹⁴ Comenius University Bratislava, Faculty of Mathematics, Physics and Informatics, Bratislava, Slovakia
- ¹⁵ COMSATS University Islamabad, Islamabad, Pakistan
- ¹⁶ Creighton University, Omaha, Nebraska, United States
- ¹⁷ Department of Physics, Aligarh Muslim University, Aligarh, India
- ¹⁸ Department of Physics, Pusan National University, Pusan, Republic of Korea
- ¹⁹ Department of Physics, Sejong University, Seoul, Republic of Korea
- ²⁰ Department of Physics, University of California, Berkeley, California, United States
- ²¹ Department of Physics, University of Oslo, Oslo, Norway
- ²² Department of Physics and Technology, University of Bergen, Bergen, Norway
- ²³ Dipartimento di Fisica dell’Università ‘La Sapienza’ and Sezione INFN, Rome, Italy
- ²⁴ Dipartimento di Fisica dell’Università and Sezione INFN, Cagliari, Italy
- ²⁵ Dipartimento di Fisica dell’Università and Sezione INFN, Trieste, Italy
- ²⁶ Dipartimento di Fisica dell’Università and Sezione INFN, Turin, Italy
- ²⁷ Dipartimento di Fisica e Astronomia dell’Università and Sezione INFN, Bologna, Italy
- ²⁸ Dipartimento di Fisica e Astronomia dell’Università and Sezione INFN, Catania, Italy
- ²⁹ Dipartimento di Fisica e Astronomia dell’Università and Sezione INFN, Padova, Italy
- ³⁰ Dipartimento di Fisica ‘E.R. Caianiello’ dell’Università and Gruppo Collegato INFN, Salerno, Italy
- ³¹ Dipartimento DISAT del Politecnico and Sezione INFN, Turin, Italy
- ³² Dipartimento di Scienze e Innovazione Tecnologica dell’Università del Piemonte Orientale and INFN Sezione di Torino, Alessandria, Italy
- ³³ Dipartimento Interateneo di Fisica ‘M. Merlin’ and Sezione INFN, Bari, Italy
- ³⁴ European Organization for Nuclear Research (CERN), Geneva, Switzerland
- ³⁵ Faculty of Electrical Engineering, Mechanical Engineering and Naval Architecture, University of Split, Split, Croatia
- ³⁶ Faculty of Engineering and Science, Western Norway University of Applied Sciences, Bergen, Norway
- ³⁷ Faculty of Nuclear Sciences and Physical Engineering, Czech Technical University in Prague, Prague, Czech Republic
- ³⁸ Faculty of Science, P.J. Šafárik University, Košice, Slovakia
- ³⁹ Frankfurt Institute for Advanced Studies, Johann Wolfgang Goethe-Universität Frankfurt, Frankfurt, Germany
- ⁴⁰ Gangneung-Wonju National University, Gangneung, Republic of Korea
- ⁴¹ Gauhati University, Department of Physics, Guwahati, India
- ⁴² Helmholtz-Institut für Strahlen- und Kernphysik, Rheinische Friedrich-Wilhelms-Universität Bonn, Bonn, Germany
- ⁴³ Helsinki Institute of Physics (HIP), Helsinki, Finland
- ⁴⁴ High Energy Physics Group, Universidad Autónoma de Puebla, Puebla, Mexico
- ⁴⁵ Hiroshima University, Hiroshima, Japan
- ⁴⁶ Hochschule Worms, Zentrum für Technologietransfer und Telekommunikation (ZTT), Worms, Germany
- ⁴⁷ Horia Hulubei National Institute of Physics and Nuclear Engineering, Bucharest, Romania
- ⁴⁸ Indian Institute of Technology Bombay (IIT), Mumbai, India
- ⁴⁹ Indian Institute of Technology Indore, Indore, India
- ⁵⁰ Indonesian Institute of Sciences, Jakarta, Indonesia
- ⁵¹ INFN, Laboratori Nazionali di Frascati, Frascati, Italy
- ⁵² INFN, Sezione di Bari, Bari, Italy
- ⁵³ INFN, Sezione di Bologna, Bologna, Italy
- ⁵⁴ INFN, Sezione di Cagliari, Cagliari, Italy
- ⁵⁵ INFN, Sezione di Catania, Catania, Italy
- ⁵⁶ INFN, Sezione di Padova, Padova, Italy
- ⁵⁷ INFN, Sezione di Roma, Rome, Italy
- ⁵⁸ INFN, Sezione di Torino, Turin, Italy
- ⁵⁹ INFN, Sezione di Trieste, Trieste, Italy

- 60 Inha University, Incheon, Republic of Korea
- 61 Institut de Physique Nucléaire d'Orsay (IPNO), Institut National de Physique Nucléaire et de Physique des Particules (IN2P3/CNRS), Université de Paris-Sud, Université Paris-Saclay, Orsay, France
- 62 Institute for Nuclear Research, Academy of Sciences, Moscow, Russia
- 63 Institute for Subatomic Physics, Utrecht University/Nikhef, Utrecht, Netherlands
- 64 Institute of Experimental Physics, Slovak Academy of Sciences, Košice, Slovakia
- 65 Institute of Physics, Homi Bhabha National Institute, Bhubaneswar, India
- 66 Institute of Physics of the Czech Academy of Sciences, Prague, Czech Republic
- 67 Institute of Space Science (ISS), Bucharest, Romania
- 68 Institut für Kernphysik, Johann Wolfgang Goethe-Universität Frankfurt, Frankfurt, Germany
- 69 Instituto de Ciencias Nucleares, Universidad Nacional Autónoma de México, Mexico City, Mexico
- 70 Instituto de Física, Universidade Federal do Rio Grande do Sul (UFRGS), Porto Alegre, Brazil
- 71 Instituto de Física, Universidad Nacional Autónoma de México, Mexico City, Mexico
- 72 iThemba LABS, National Research Foundation, Somerset West, South Africa
- 73 Johann-Wolfgang-Goethe Universität Frankfurt Institut für Informatik, Fachbereich Informatik und Mathematik, Frankfurt, Germany
- 74 Joint Institute for Nuclear Research (JINR), Dubna, Russia
- 75 Korea Institute of Science and Technology Information, Daejeon, Republic of Korea
- 76 KTO Karatay University, Konya, Turkey
- 77 Laboratoire de Physique Subatomique et de Cosmologie, Université Grenoble-Alpes, CNRS-IN2P3, Grenoble, France
- 78 Lawrence Berkeley National Laboratory, Berkeley, California, United States
- 79 Lund University Department of Physics, Division of Particle Physics, Lund, Sweden
- 80 Nagasaki Institute of Applied Science, Nagasaki, Japan
- 81 Nara Women's University (NWU), Nara, Japan
- 82 National and Kapodistrian University of Athens, School of Science, Department of Physics, Athens, Greece
- 83 National Centre for Nuclear Research, Warsaw, Poland
- 84 National Institute of Science Education and Research, Homi Bhabha National Institute, Jatni, India
- 85 National Nuclear Research Center, Baku, Azerbaijan
- 86 National Research Centre Kurchatov Institute, Moscow, Russia
- 87 Niels Bohr Institute, University of Copenhagen, Copenhagen, Denmark
- 88 Nikhef, National institute for subatomic physics, Amsterdam, Netherlands
- 89 NRC Kurchatov Institute IHEP, Protvino, Russia
- 90 NRC Kurchatov Institute - ITEP, Moscow, Russia
- 91 NRNU Moscow Engineering Physics Institute, Moscow, Russia
- 92 Nuclear Physics Group, STFC Daresbury Laboratory, Daresbury, United Kingdom
- 93 Nuclear Physics Institute of the Czech Academy of Sciences, Řež u Prahy, Czech Republic
- 94 Oak Ridge National Laboratory, Oak Ridge, Tennessee, United States
- 95 Ohio State University, Columbus, Ohio, United States
- 96 Petersburg Nuclear Physics Institute, Gatchina, Russia
- 97 Physics department, Faculty of science, University of Zagreb, Zagreb, Croatia
- 98 Physics Department, Panjab University, Chandigarh, India
- 99 Physics Department, University of Jammu, Jammu, India
- 100 Physics Department, University of Rajasthan, Jaipur, India
- 101 Physikalisches Institut, Eberhard-Karls-Universität Tübingen, Tübingen, Germany
- 102 Physikalisches Institut, Ruprecht-Karls-Universität Heidelberg, Heidelberg, Germany
- 103 Physik Department, Technische Universität München, Munich, Germany
- 104 Politecnico di Bari, Bari, Italy
- 105 Research Division and ExtreMe Matter Institute EMMI, GSI Helmholtzzentrum für Schwerionenforschung GmbH, Darmstadt, Germany
- 106 Rudjer Bošković Institute, Zagreb, Croatia
- 107 Russian Federal Nuclear Center (VNIIEF), Sarov, Russia
- 108 Saha Institute of Nuclear Physics, Homi Bhabha National Institute, Kolkata, India
- 109 School of Physics and Astronomy, University of Birmingham, Birmingham, United Kingdom
- 110 Sección Física, Departamento de Ciencias, Pontificia Universidad Católica del Perú, Lima, Peru

- 111 Shanghai Institute of Applied Physics, Shanghai, China
- 112 St. Petersburg State University, St. Petersburg, Russia
- 113 Stefan Meyer Institut für Subatomare Physik (SMI), Vienna, Austria
- 114 SUBATECH, IMT Atlantique, Université de Nantes, CNRS-IN2P3, Nantes, France
- 115 Suranaree University of Technology, Nakhon Ratchasima, Thailand
- 116 Technical University of Košice, Košice, Slovakia
- 117 Technische Universität München, Excellence Cluster 'Universe', Munich, Germany
- 118 The Henryk Niewodniczanski Institute of Nuclear Physics, Polish Academy of Sciences, Cracow, Poland
- 119 The University of Texas at Austin, Austin, Texas, United States
- 120 Universidad Autónoma de Sinaloa, Culiacán, Mexico
- 121 Universidade de São Paulo (USP), São Paulo, Brazil
- 122 Universidade Estadual de Campinas (UNICAMP), Campinas, Brazil
- 123 Universidade Federal do ABC, Santo Andre, Brazil
- 124 University of Cape Town, Cape Town, South Africa
- 125 University of Houston, Houston, Texas, United States
- 126 University of Jyväskylä, Jyväskylä, Finland
- 127 University of Liverpool, Liverpool, United Kingdom
- 128 University of Science and Technology of China, Hefei, China
- 129 University of South-Eastern Norway, Tonsberg, Norway
- 130 University of Tennessee, Knoxville, Tennessee, United States
- 131 University of the Witwatersrand, Johannesburg, South Africa
- 132 University of Tokyo, Tokyo, Japan
- 133 University of Tsukuba, Tsukuba, Japan
- 134 Université Clermont Auvergne, CNRS/IN2P3, LPC, Clermont-Ferrand, France
- 135 Université de Lyon, Université Lyon 1, CNRS/IN2P3, IPN-Lyon, Villeurbanne, Lyon, France
- 136 Université de Strasbourg, CNRS, IPHC UMR 7178, F-67000 Strasbourg, France, Strasbourg, France
- 137 Université Paris-Saclay Centre d'Etudes de Saclay (CEA), IRFU, Département de Physique Nucléaire (DPhN), Saclay, France
- 138 Università degli Studi di Foggia, Foggia, Italy
- 139 Università degli Studi di Pavia, Pavia, Italy
- 140 Università di Brescia, Brescia, Italy
- 141 Variable Energy Cyclotron Centre, Homi Bhabha National Institute, Kolkata, India
- 142 Warsaw University of Technology, Warsaw, Poland
- 143 Wayne State University, Detroit, Michigan, United States
- 144 Westfälische Wilhelms-Universität Münster, Institut für Kernphysik, Münster, Germany
- 145 Wigner Research Centre for Physics, Budapest, Hungary
- 146 Yale University, New Haven, Connecticut, United States
- 147 Yonsei University, Seoul, Republic of Korea